

1 **Description and Evaluation of a New 4-Mode Version of Modal Aerosol Module**
2 **(MAM4) within Version 5.3 of the Community Atmosphere Model**

3
4 Xiaohong Liu^{1,2}, Po-Lun Ma¹, Hailong Wang¹, Simone Tilmes³, Balwinder Singh¹,
5 Richard C. Easter¹, Steven J. Ghan¹, and Philip J. Rasch¹

6
7 ¹ *Atmospheric Sciences and Global Change Division, Pacific Northwest National*
8 *Laboratory, Richland, Washington, USA*

9 ² *Now at Department of Atmospheric Science, University of Wyoming, Laramie,*
10 *Wyoming, USA*

11 ³ *National Center for Atmospheric Research, Boulder, Colorado, USA*

12
13
14
15
16 Corresponding author:

17
18 Xiaohong Liu
19 Department of Atmospheric Science
20 University of Wyoming
21 Dept. 3038, 1000 East University Avenue
22 Laramie, WY 82071
23 Email: xliu6@uwyo.edu

24
25 Tel: (307) 766-3225

26 Fax: (307) 766-2635

27
28
29
30

31

32

33 **Abstract**

34 Atmospheric carbonaceous aerosols play an important role in the climate system
35 by influencing the Earth's radiation budgets and modifying the cloud properties. Despite
36 the importance, their representations in large-scale atmospheric models are still crude,
37 which can influence model simulated burden, lifetime, physical, chemical and optical
38 properties, and the climate forcing of carbonaceous aerosols. In this study, we improve
39 the current 3-mode version of modal aerosol module (MAM3) in the Community
40 Atmosphere Model version 5 (CAM5) by introducing an additional primary carbon mode
41 to explicitly account for the microphysical ageing of primary carbonaceous aerosols in
42 the atmosphere. Compared to MAM3, the 4-mode version of MAM (MAM4)
43 significantly increases the column burdens of primary particulate organic matter (POM)
44 and black carbon (BC) by up to 40% in many remote regions, where in-cloud scavenging
45 plays an important role in determining the aerosol concentrations. Differences in the
46 column burdens for other types of aerosol (e.g., sulfate, secondary organic aerosols,
47 mineral dust, sea salt) are less than 1%. Evaluating the MAM4 simulation against in situ
48 surface and aircraft observations, we find that MAM4 significantly improves the
49 simulation of seasonal variation of near-surface BC concentrations in the polar regions,
50 by increasing the BC concentrations in all seasons and particularly in cold seasons.
51 However, it exacerbates the overestimation of modeled BC concentrations in the upper
52 troposphere in the Pacific regions. The comparisons suggest that, to address the
53 remaining model POM and BC biases, future improvements are required related to (1) in-
54 cloud scavenging and vertical transport in convective clouds and (2) emissions of
55 anthropogenic and biomass burning aerosols.

56

57 **1. Introduction**

58 Atmospheric aerosols from natural and anthropogenic sources play an important
59 role in the climate system. In spite of extensive studies in the past several decades,
60 radiative forcing of atmospheric aerosols is still associated with large uncertainties
61 according to the Intergovernmental Panel of Climate Change Assessment Reports
62 (Forster et al., 2007; Myhre et al., 2013). The large uncertainty of aerosol radiative
63 forcing among global climate models (GCMs) reflects the diversity in treatments of
64 aerosol properties and processes in GCMs. A multitude of processes influence aerosols in
65 the atmosphere, which include emission, nucleation, coagulation, gas-phase and aqueous
66 chemical reactions, dry deposition, gravitational settling, and wet scavenging by clouds
67 and precipitation. These processes determine the burden and lifetime of aerosols, particle
68 size distribution, mixing state, and thus the radiative forcing of aerosols on the climate
69 (Textor et al., 2006; Schulz et al., 2006; Quaas et al., 2009). Furthermore, the burden and
70 size distribution of aerosols control their surface area density and thereby influence
71 heterogeneous chemistry, which can then induce chemical effects such as extended
72 methane lifetime (Tilmes et al., 2015).

73 Primary carbonaceous aerosols are produced from the incomplete combustion of
74 fossil and biomass fuels, and are one of the most important types of aerosol in the
75 atmosphere. Most models tend to speciate the mass of carbonaceous aerosols into a light-
76 absorbing component (black carbon, BC) and a purely-scattering component (particulate
77 organic matter, POM). BC has a strong warming effect, second only to carbon dioxide on
78 the climate system, with the industrial-era (1750 to 2005) direct radiative forcing of
79 $+0.71 \text{ W m}^{-2}$ with 90% uncertainty bounds of $(+0.08, +1.27) \text{ W m}^{-2}$ (Bond et al., 2013).

80 Once emitted into the atmosphere, BC can be transported to the polar regions far from
81 distant sources (e.g., Bian et al., 2013; H. Wang et al., 2013), and deposited on the
82 surface of snow and sea ice by dry and wet deposition (e.g., Jiao et al., 2014). BC-in-
83 snow can absorb solar radiation efficiently, heat the snowpack, and induce a positive
84 feedback on the surface albedo (Hansen and Nazarenko, 2004; Jacobson, 2004; Hansen et
85 al., 2005; Flanner et al., 2007, 2009, 2012).

86 Although climatologically important, BC is still not simulated well by GCMs in
87 many regions. For example, high bias of BC concentrations in the upper troposphere in
88 the tropics and subtropics exists in almost all the global models participating in the
89 AeroCom Phase I and Phase II intercomparison (Koch et al., 2009; Schwarz et al., 2010;
90 Samset et al., 2014), while low BC bias in the lower atmosphere by over a factor of 10
91 exists in the polar regions. The aerosol absorption optical depth also tends to be biased
92 low in GCMs compared to satellite observations (Koch et al., 2009), although compares
93 better to ground-based sun photometers (Kinne et al., 2006). Note that differences
94 between satellite retrievals and ground-based observations can be attributed to
95 collocation/sampling and/or retrieval errors, but require further investigation.

96 Freshly emitted carbonaceous aerosols are usually hydrophobic, especially those
97 emitted from fossil fuel combustion. They cannot serve as cloud condensation nuclei
98 (CCN). However, these particles can experience physical and chemical ageing in the
99 atmosphere. Condensation and coagulation processes coat carbonaceous particles with
100 soluble species (e.g., sulfate), which enables them to nucleate cloud droplets. Inside
101 clouds, once these cloud droplets are converted to raindrops via various rain-production
102 processes, carbonaceous aerosols in the cloud droplets can be removed from the

103 atmosphere when raindrops fall to the ground (i.e., the so-called nucleation scavenging).
104 Meanwhile, when BC is internally mixed with non-absorbing soluble materials, its
105 absorption of sunlight can be enhanced compared to the external mixing treatment, as the
106 soluble materials act as a lens (for the shell-core representation of particle morphology)
107 (Jacobson 2001, 2003) or expand the cross section of the absorbing material (for the
108 volume mixing representation) (Adachi et al., 2010). Therefore, in order to simulate
109 aerosol concentration, spatial distribution, lifetime, and climate forcing correctly, a
110 physically based representation of atmospheric processes affecting the mixing state of
111 carbonaceous aerosols is needed in the models.

112 The simplest treatment of carbonaceous aerosols, e.g., bulk models, assumes that
113 carbonaceous aerosols and other aerosol types (e.g., sulfate) are externally mixed (i.e.,
114 different components do not coexist in the same particle), and often uses a prescribed
115 time scale (1-2 days) for the ageing of primary carbonaceous aerosols from the
116 hydrophobic to hydrophilic state (Cooke and Wilson, 1996; Tie et al., 2005). More
117 sophisticated treatments, e.g., modal and sectional aerosol models, predict the aerosol
118 size distribution, and determine the mixing state of carbonaceous aerosols by the coating
119 thickness of soluble materials such as sulfate and organics on these aerosols (e.g., Liu et
120 al., 2005; Stier et al., 2005; Spracklen et al., 2005; Bauer et al., 2008). Even more
121 advanced aerosol treatments explicitly resolve the mixing state by tracking the
122 composition of individual particles in a population of different aerosol types (Riemer et
123 al., 2009). However, this approach is computationally prohibitive for global models.

124 Liu et al. (2012) developed a modal aerosol module (MAM) for the Community
125 Atmosphere Model version 5 (CAM5). The 7-mode version of MAM (MAM7) provides

126 the benchmark simulation of aerosols in CAM5. In MAM7, the microphysical ageing of
127 primary carbonaceous aerosols from the primary carbon mode to the accumulation mode
128 through condensation and coagulation is explicitly treated, with a threshold coating
129 thickness of three monolayers of sulfate. For the sake of computational efficiency, a
130 simplified 3-mode version of MAM (MAM3) was developed for use as the default in
131 CAM5. MAM3 is based on the MAM7 by merging the primary carbon mode with the
132 accumulation mode, and assuming instantaneous internal mixing of primary
133 carbonaceous aerosols with secondary aerosols (e.g., sulfate and secondary organic
134 aerosols).

135 CAM5 with MAM3 is able to simulate many features of the observed spatial
136 distribution of concentrations of different types of aerosol, aerosol optical depth, aerosol
137 number and size distribution over different geographical regions of the world. However,
138 similar to other global models (Koch et al., 2009), CAM5 significantly underestimates
139 the near-surface BC concentrations in remote regions, e.g., in the Arctic (Liu et al., 2012;
140 H. Wang et al., 2013; Ma et al., 2013a). While the underestimation of BC emission in
141 Asia (e.g., Cohen and Wang, 2014) and in the high latitudes of the northern hemisphere
142 (NH) (e.g., Stohl et al., 2013) can be an important factor, the excessively efficient
143 scavenging of BC by liquid cloud processes (H. Wang et al., 2013) and the coarse
144 horizontal resolution (~100-200 km) of the model (Ma et al., 2014) also contribute to this
145 model bias.

146 To address this low BC bias found in CAM5 with MAM3 as well as in many
147 GCMs, without significantly increasing the computational cost, we have developed a 4-
148 mode version of MAM (MAM4) for the next generation of GCMs, including the version

149 6 of CAM (CAM6) and the U.S. Department of Energy's Accelerated Climate Modeling
150 for Energy (ACME).

151 In this paper, we provide a technical description and a first evaluation of MAM4.
152 The paper is organized as follows. Section 2 describes MAM4. Section 3 introduces the
153 sensitivity tests related to the microphysical ageing of primary carbonaceous aerosols and
154 model horizontal resolution. Comparison of MAM4 with MAM3 and evaluation of
155 MAM4 with observation data focusing on BC are given in section 4. Conclusions are
156 drawn in section 5.

157

158 **2. Model Description**

159

160 2.1 CAM5

161

162 CAM5 is the atmosphere component of the Community Earth System Model
163 version 1 (CESM1.0) (Neale et al., 2012). Compared to its earlier versions, CAM5 is
164 designed to simulate aerosol effects on stratiform clouds (i.e., indirect effect) through
165 acting as CCN and ice nuclei (IN). Aerosol effects on convective cloud microphysics are
166 not treated in CAM5. MAM predicts the mass mixing ratios of internally mixed aerosol
167 species within an aerosol mode and number concentrations of aerosol in that mode (Liu et
168 al., 2012). A two-moment stratiform cloud microphysics scheme (Morrison and
169 Gettelman, 2008; Gettelman et al., 2010) predicts the mass and number mixing ratios of
170 cloud liquid and cloud ice, diagnoses the mass and number mixing ratios of rain and
171 snow, and considers the complicated conversions among the cloud hydrometeors. The
172 nucleation (i.e., in-cloud) scavenging of aerosols in stratiform clouds is treated
173 consistently with the droplet activation in cloud microphysics (Abdul-Razzak and Ghan,

174 2000), by explicitly calculating aerosols in the cloud-liquid-borne state (Ghan and Easter,
175 2006). Aerosols can affect ice microphysics by homogeneous ice nucleation of aerosol
176 solution droplets (e.g., sulfate aerosol) in cirrus clouds with temperatures lower than
177 about -37 °C and heterogeneous ice nucleation in cirrus clouds and in mixed-phase clouds
178 (Liu et al., 2007; Liu and Penner, 2005). However, aerosol scavenging by these ice
179 nucleation processes is neglected in CAM5.

180 Other major components in CAM5 include (1) a stratiform cloud macrophysics
181 scheme (Park et al., 2014) to estimate the cloudy volume (cloud fraction), (2) a moist
182 turbulence scheme (Bretherton and Park, 2009) to explicitly simulate stratus-radiation-
183 turbulence interactions, (3) a radiation scheme (Iacono et al., 2008) to more accurately
184 treat the radiative effects of clouds and aerosol, (4) a shallow convection scheme (Park
185 and Bretherton, 2009) to better simulate the observed spatial distribution of shallow
186 convective activity, and (5) a modified deep convection scheme (Zhang and McFarlane,
187 1995) with the inclusion of sub-grid convective momentum transports (Richter and
188 Rasch, 2008) and the updated closure (Neale et al., 2008).

189 190 2.2 MAM in CAM5

191
192 There are two versions of MAM available in CAM5: the default MAM3 and an
193 optional MAM7 (Liu et al., 2012). MAM3 predicts the aerosol size distribution with three
194 aerosol modes (Aitken, accumulation and coarse modes), while MAM7 includes seven
195 aerosol modes (Aitken, accumulation, primary carbon, fine dust and fine sea salt, coarse
196 dust and coarse sea salt modes). In MAM3 instantaneous ageing of primary carbonaceous
197 particles is assumed by emitting them in the accumulation mode, while in MAM7 the
198 ageing of the carbonaceous particles in the primary carbon mode due to the condensation

199 of sulfuric acid (H_2SO_4 vapor), ammonia (NH_3), and the semi-volatile organics, and the
200 coagulation of Aitken mode particles with primary-carbon mode particles are explicitly
201 treated. Both sea salt and dust emissions are calculated on-line and are highly sensitive to
202 the surface wind speed. Other processes in the atmosphere affecting aerosol properties
203 (e.g., number/mass concentration, size, density, refractive index, chemical composition)
204 include new particle formation, gas- and aqueous-phase chemistry, dry deposition and
205 gravitational settling, water uptake, in-cloud (nucleation) and below-cloud scavenging,
206 and release from evaporated cloud and rain drops. There are 15 transported aerosol
207 tracers in MAM3 and 31 in MAM7.

208
209

210 2.3 Development of MAM4

211 In this study, we developed a 4-mode version of MAM (MAM4), which includes
212 an additional primary carbon mode on top of MAM3 to explicitly treat the microphysical
213 ageing of primary carbonaceous aerosols in the atmosphere. As in MAM7, fresh emitted
214 POM/BC particles are put in the newly added primary carbon mode. A criterion of 8
215 mono-layers of sulfate or equivalent amount of secondary organic aerosol (SOA) with the
216 same increase in volume-weighted hygroscopicity as sulfate is required to convert
217 POM/BC particles in the primary carbon mode to the accumulation mode. We use a value
218 of 0 for the hygroscopicity (κ parameter) of POM from all sources. This value is more
219 representative of POM produced from fossil fuel combustion. The hygroscopicity of
220 POM from biomass burning source can be higher (0.06-0.30) (Liu and Wang, 2010). A
221 non-zero hygroscopicity of POM allows in-cloud scavenging of POM/BC particles in the
222 primary carbon mode before they are aged into the accumulation mode, and then the

223 differences in the POM/BC concentrations between MAM3 and MAM7 are smaller (Liu
224 et al., 2012). A separate treatment of carbonaceous aerosols emitted from fossil fuel
225 versus biomass burning sources will be needed to seamlessly consider the different
226 hygroscopicity of POM. The κ value for BC is set to 0 to reflect its hydrophobic nature.

227 Similarly, the refractive index for BC-containing particles changes as the particles
228 age. The refractive index for fresh particles is the volume mean of the refractive index of
229 the BC and POM, while the refractive index of aged particles is the volume mean of the
230 refractive index of all components of the accumulation mode.

231 With the new primary carbon mode, three prognostic variables are added in
232 MAM4 compared to MAM3: mass mixing ratios of POM and BC in the primary carbon
233 mode and number concentration of the primary carbon mode particles, which brings the
234 total number of aerosol tracers from 15 in MAM3 to 18 in MAM4. The other aerosol
235 tracers and precursor gases are the same as those in MAM3. The computational cost
236 increases by $\sim 10\%$ for the stand-alone CAM5 (i.e., an uncoupled atmosphere-only
237 simulation with prescribed sea surface temperatures and sea ice) with MAM4 compared
238 to CAM5 with MAM3. As noted in Liu et al. (2012), CAM5 with MAM7 is 30% slower
239 than CAM5 with MAM3. Figure 1 shows the schematic of aerosol modes and associated
240 aerosol tracers in MAM4.

241

242 **3. Model Configurations and Experiments**

243 Two sets of experiments were performed using version 5.3 of CAM (CAM5.3)
244 with the new MAM4 (hereafter CAM5-MAM4), as listed in Table 1. The first set is to
245 test the model sensitivity to the criterion of number of mono-layers required for the
246 ageing of POM/BC particles from the primary carbon mode to the accumulation mode.

247 We conducted four experiments with the number of mono-layers set to 1, 2, 4 and 8,
248 respectively. A higher mono-layer criterion means that a larger sulfate or SOA coating
249 thickness is needed to age the primary carbonaceous aerosols, and thus these particles
250 will stay longer in the primary carbon mode before converting to the accumulation mode.
251 As noted in Liu et al. (2012), for a non-hygroscopic particle with a 0.134 μm diameter,
252 which is the volume-mean size for BC/POM emissions, the critical supersaturation in the
253 case of 8 mono-layers of sulfate is 0.32% based on the Köhler theory, in comparison to
254 0.49% in the case of 3 mono-layers. These CAM5-MAM4 simulations were conducted
255 for present-day (year 2000) emissions and climate conditions with freely evolving
256 meteorological fields (e.g., winds and temperature) at $0.9^\circ \times 1.25^\circ$ (1° hereafter) horizontal
257 resolution for 11 years. The last 10-year results are used for analysis. For comparison, an
258 additional experiment using CAM5.3 with the default MAM3 was performed for 11 years
259 at the same 1° horizontal resolution. We also conducted an experiment with MAM7,
260 which gave BC and POM results very similar to MAM4 (Figure not shown), and thus are
261 not included in the comparison.

262 The second set of experiments is to test the model sensitivity to the horizontal
263 resolution (see Table 1), since model resolution has been suggested to play an important
264 role for the BC transport to the remote regions (Ma et al., 2013a, 2014). Four experiments
265 were conducted at $1.9^\circ \times 2.5^\circ$ (2° hereafter), 1° , 0.5° , and 0.25° using the specified
266 dynamics (SD) configuration (also known as the nudging technique) where the model
267 meteorology is strongly constrained by an external meteorological analysis (Ma et al.,
268 2013a, 2013b, 2015; Tilmes et al., 2015). To explore the behavior of MAM4 at higher
269 horizontal resolution, we used the ECMWF Year of Tropical Convection (YOTC) high-

270 resolution (0.15°) analysis to drive the model, while aerosol emissions are the same as
271 that in the first set of experiments. The SD configuration has been recalibrated so that the
272 model physics properly responds to the realistic meteorology (Ma et al., 2015). This
273 approach facilitates the direct comparison between model simulations and field campaign
274 measurements since the simulation of aerosol lifecycle (emission, transport, and
275 deposition) is based on a realistic climate. These SD simulations were performed from 1
276 November 2008 to 1 January 2010, and the one-year results in 2009 were used for our
277 analysis. The 8-monolayer criterion was used in this set of experiments. In addition, by
278 comparing the second set of experiments with the SD configuration to the first set of
279 experiments with the free-running configuration (e.g., MAM4L8 versus MAM4R1), we
280 can examine the effect of model meteorology on aerosol simulations. We also ran
281 CAM5.3 with the default MAM3 at 1° resolution with the SD configuration for
282 comparison.

283

284 **4. Results**

285 *4.1 Comparison of MAM4 with MAM3*

286 Figure 2 shows the latitudinal and longitudinal distributions of annual mean
287 column burdens of BC and POM from the set 1 experiments with CAM5-MAM4, in
288 comparison with the default MAM3. BC and POM burdens have maxima in industrial
289 regions (e.g., East Asia, Europe, and North America) and in biomass burning regions
290 (e.g., Central and Southern Africa, South America, Indonesia, and Siberia), but a small
291 fraction of BC and POM is transported to the Pacific and Atlantic Oceans, and to the
292 Arctic. In general the Southern Hemisphere (SH) high-latitudes have the lowest BC and

293 POM burdens. As expected, BC and POM burdens from CAM5-MAM4 simulations are
294 much higher than those with MAM3 far from source regions. The increase in BC and
295 POM burdens with MAM4 is most evident for the largest number of monolayers. This is
296 more clearly seen in Figure 3, which shows the relative (percentage) differences of
297 annual mean burdens of BC and POM between MAM4 and MAM3 for the set 1
298 experiments. Compared to MAM3, the global total burden increase for MAM4L1 is 10%
299 and 16%, respectively for BC and POM, while it is 128% and 174% for MAM4L8. The
300 largest increase occurs over the remote oceans and polar regions where the background
301 concentrations are low (see Figure 2). An increase by up to a factor of 10 can be seen in
302 the Arctic in the MAM4L8 case. In contrast, the increase is less than a factor of 2 (i.e.,
303 less than 100%) in the regions over the continents where the major sources are. For a
304 larger threshold number of mono-layers, carbonaceous aerosols stay longer in the primary
305 carbon mode, indicating a slower ageing. Aerosol particles in the primary carbon mode
306 are subject to relatively inefficient impaction scavenging by precipitating hydrometeors
307 but are not subject to in-cloud scavenging, which allows more POM/BC to be transported
308 to the remote regions. We note that non-carbonaceous aerosols (i.e., sulfate, SOA,
309 mineral dust and sea salt) are affected very little (i.e., ~1% difference for dust, and less
310 than 0.5% difference for other aerosol species, which are about an order of magnitude
311 smaller than their interannual variabilities) by the introduction of the primary carbon
312 mode. The number of CCN at 0.1% supersaturation, which is important for the cloud
313 formation and climate, changes by ~6% on the global mean.

314 Figure 4 shows the latitudinal and longitudinal distributions of annual mean BC
315 and POM column burdens from the set 2 experiments. With an increase of the horizontal

316 resolution from 2° to 0.25° for CAM5-MAM4 simulations, BC and POM burdens both
317 increase by 10-20% on the global mean and by about a factor of 2 in the Antarctic. This
318 increase is due to (1) the resolved meso-scale eddies at higher resolutions which leads to
319 stronger poleward eddy transport of aerosol species, and (2) less frequent wet scavenging
320 resulting from the reduced frequency of collocation between aerosols and clouds at
321 higher resolutions (Ma et al., 2014). Figure 5 shows the percentage differences of annual
322 mean BC and POM burdens at 1° , 0.5° , and 0.25° relative to 2° for the set 2 experiments
323 with CAM5-MAM4. With the increase of horizontal resolution, clearly more BC and
324 POM are transported to the remote regions. The largest increase occurs in the Antarctic
325 by up to a factor of 2. Other strong increases are seen in regions away from major sources,
326 such as the Arctic, western and eastern Pacific, East Asian and North American pollution
327 outflow regions, indicating the enhanced transport out of the source regions at higher
328 resolutions. The resolution sensitivity of BC and POM, as well as other aerosols, can
329 contribute to the resolution sensitivity of aerosol-cloud interactions such as the enhanced
330 but less frequent droplet nucleation due to stronger subgrid vertical velocity, reduced
331 collocation of aerosols and clouds, and higher aerosol concentration (Ma et al., 2015).
332 The regions with the smallest relative increases are the POM/BC source regions (e.g.,
333 East Asia, Southern Africa, South America), and the subtropical dry zones where cloud
334 and precipitation scavenging of aerosols is relatively weak.

335 By comparing MAM4L8 (in Figure 2) with MAM4R1 (in Figure 4), all else being
336 the same, CAM5 with the one-year specific dynamics gives $\sim 20\%$ lower BC and POM
337 global burdens than the 10-year free-running simulation. This can be partly attributed to
338 the inter-annual variability of aerosols in the MAM4L8 simulation. However, the primary

339 cause of this difference is the different meteorological conditions between the SD and the
340 free-running CAM5 that affect the transport and cloud processing of aerosols.

341

342 *4.2 Annual global budgets of BC and POM*

343 Tables 2 and 3 give the BC and POM budgets, respectively, for the sensitivity to
344 the number of monolayers in the set 1 experiments. Most BC is removed from the
345 atmosphere by wet deposition (~80%). When the number of monolayers required for
346 microphysical ageing of BC from the primary carbon mode to the accumulation mode is
347 increased, the contribution of wet deposition to the total BC sink decreases somewhat and
348 the contribution of dry deposition increases. Most BC resides in the accumulation mode,
349 indicating the relatively fast ageing of BC after it is emitted into the primary carbon mode.
350 The ageing timescale of primary carbon mode BC (i.e., burden divided by the ageing flux
351 from primary carbon mode to the accumulation mode) ranges from 0.24 days in
352 MAM4L1 to 2.08 days in MAM4L8. With more monolayers and slower ageing of
353 primary carbonaceous aerosols, more emitted BC remains in the primary carbon mode,
354 and is not subject to cloud processing. For example, about 30% of the total BC burden is
355 in the primary carbon mode for the MAM4L8 experiment, compared to 6% for the
356 MAM4L1 experiment. The total BC burden increases from 0.087 (MAM4L1) to 0.123
357 Tg (MAM4L8), because the BC lifetime increases from 4.10 (MAM4L1) to 5.79 days
358 (MAM4L8). Interestingly, BC burden in the accumulation mode does not change much in
359 these simulations, because the accumulation mode BC source (from ageing) and lifetime
360 do not change much as the ageing criterion (monolayers) changes (Liu et al., 2012).

361 Similar results can be derived for POM (Table 3), except that POM emissions are
362 ~6 times higher, and the burdens are 7-8 times higher than those of BC in these
363 simulations. The longer lifetime of POM than that of BC reflects different spatial and
364 temporal distributions of POM versus BC emissions from different sources (e.g., fossil
365 fuel and biomass burning) with respect to cloud and precipitation distributions. A higher
366 percentage of POM is emitted from biomass burning emissions than for BC, and the
367 biomass burning emissions tend to occur more in tropical dry seasons and boreal non-
368 winter seasons. Also, it is assumed that POM/BC from biomass burning emissions is
369 injected into higher altitudes (up to 6 km) and thus is subject less to wet removal by
370 clouds, compared to the POM/BC from fossil fuel, which is emitted near the surface. The
371 inter-annual variation of modeled BC/POM due to natural variability (i.e., BC/POM
372 difference among different years of 10-year climatology) is quantified to be very small,
373 as indicated by the standard deviations of BC/POM budget terms about the 10-year mean
374 in Tables 2 and 3 for the set 1 experiments.

375 Tables 4 and 5 give the BC and POM budgets, respectively, for the set 2
376 experiments. BC and POM burdens increase by 12% and 7%, respectively, from 2° to
377 0.25°, with the increase occurring in the accumulation mode. The nearly invariant POM
378 and BC burdens in the primary carbon mode with resolution indicate that the
379 microphysical ageing of primary carbonaceous aerosols is insensitive to the resolution.
380 This is verified by the nearly constant ageing timescales of primary carbon mode POM
381 and BC. The accumulation mode burden increases are due to longer lifetimes for the
382 accumulation mode aerosol (e.g., 3.38 days versus 3.95 days for BC at 2° versus 0.25°
383 resolution). This is due to slower wet removal rates (i.e., wet deposition sinks divided by

384 burdens) at higher resolution, even though the absolute wet removal sinks are slightly
385 greater at higher resolution, and the dry deposition sinks are correspondingly slightly
386 lower. Specified dynamics (MAM4R1) reduces BC and POM burdens by 18% and 14%,
387 respectively, compared to free running (MAM4L8), with most of the decrease occurring
388 in the accumulation mode.

389

390 *4.3 Comparison with in situ observations*

391 Next, we compare the simulations with a dataset obtained during the HIAPER
392 (High-Performance Instrumented Airborne Platform for Environmental Research) Pole-
393 to-Pole Observations (HIPPO) campaigns (HIPPO 1-5) over the remote Pacific from
394 80 °N to 67 °S in January and November 2009, March/April 2010, and June/July and
395 August/September 2011 (Wofsy et al., 2011). Tilmes et al. (2015) evaluated CAM5 with
396 MAM3 against these campaigns, so in this study we focus on evaluating MAM4 results.
397 Figure 6 shows the latitude-altitude cross section of the Single Particle Soot Photometer
398 (SP2) measured BC concentrations during the HIPPO 1-5 campaigns (Schwarz et al.,
399 2013), in comparison with CAM5-MAM4 simulated BC concentrations for the same time
400 periods in the set 2 experiments. Here we only show model simulations from the set 2
401 experiments where meteorological fields from the YOTC analysis are used to drive the
402 model simulations. Note that the aerosol emissions used in this study are the present-day
403 emissions (i.e., from the year 2000), so the inter-annual variability of emissions
404 (especially for biomass burning emissions) is not accounted for. The highest observed BC
405 concentrations were in March/April 2010 in the NH mid-latitudes, resulting from strong
406 transport of BC from the East Asian continents to the Pacific (Gao et al., 2014).

407 Observed BC concentrations in the NH were lowest in August/September compared to
408 other seasons, consistent with the strong wet scavenging of aerosols by the East Asian
409 monsoon precipitation in the summer. Elevated BC concentrations in the NH high
410 latitudes (e.g., Arctic) can be seen throughout the seasons, most evident in the spring time
411 (March/April), with the maximum BC concentrations at 3-7 km, due to the transport from
412 the NH mid-latitudes (H. Liu et al., 2011; H. Wang et al., 2013; Ma et al., 2013; Bian et
413 al., 2014). BC concentrations in the SH over $\sim 50^{\circ}\text{S}$ had a maximum in August/
414 September 2011, and were produced from South American and Australian biomass
415 burning activities in the dry season. The poleward transport of BC in SH can also be seen
416 at high altitudes over 5 km, particularly during August/September.

417 CAM5-MAM4 running at the four model resolutions is able to capture the
418 maximum of BC concentrations in the NH mid-latitudes in March/April 2010. MAM4
419 shows a better agreement with the HIPPO measurements compared with MAM3 (Tilmes
420 et al., 2015); however, the magnitude is still too low. This could be attributed to the
421 underestimation of BC emissions in East Asia in the IPCC AR5 emission inventory used
422 in CAM5 (Lamarque et al., 2010), as reported by previous studies (e.g., Cohen and Wang,
423 2014). We also find that the simulated aerosol layers are at higher altitudes than the
424 observations. The maximum of BC concentrations in MAM4 is generally between 5 and
425 10 km, suggesting that the model still has deficiency in the treatment of convective
426 transport and scavenging of aerosols in CAM5 (H. Wang et al., 2013). Excessive BC
427 aloft was also found in the HadGEM3–UKCA model and was attributed to the coupling
428 of convective transport and convective scavenging (Kipling et al., 2013). This bias is
429 also evident in model simulations in June/July and August/September 2011. Overall, the

430 model overestimates BC concentrations in the upper troposphere. With the increase of
431 model resolution more BC is transported to the polar regions, but increases occur
432 primarily in the upper troposphere and lower stratosphere and is particularly noticeable in
433 January 2009.

434 Figures 7 and 8 compare the modeled BC profiles from the various CAM5
435 simulations in set 1 and 2 experiments, respectively, with SP2 measured BC profiles
436 during the HIPPO1 campaign over the Arctic and remote Pacific in January 2009
437 (Schwarz et al., 2010). It is worth noting that the 10-year average from our set 1
438 experiments is viewed as an ensemble mean from 10 realizations, representing the free-
439 running model's present-day BC climatology, while the observations represent BC in
440 specific years (which depend on the specific observations). In contrast, our set 2
441 experiments are nudged toward the year 2009 meteorology. The differences in BC from
442 MAM4L8 of set 1 and MAM4R1 of set 2 are due to differences in their meteorology
443 (winds, clouds, and precipitation), which include the differences between a 10 year
444 average (or ensemble) and a single year, as well as the differences between the free-
445 running model's meteorology and the nudged model's meteorology (which is very close
446 to the reanalysis).

447 As seen in Figure 7, vertical profiles of observed mean BC concentrations show
448 strong variability with latitude zones, and standard deviations of observed BC
449 concentrations are also large. The observations show that BC concentrations increase
450 with altitude in the SH high latitudes (60-67 °S), indicating the poleward transport of BC
451 in the upper troposphere by the general circulation. At mid-latitudes (20-60 °N and 20-60
452 °S), less vertical variation is observed. In the tropics (20°S-20°N), BC concentrations

453 increase with altitude and reach a maximum near 700 hPa, likely from biomass burning,
454 and then reduce rapidly with height. Over the NH high latitudes (60-80 °N), a steady
455 decreasing trend with height is found. All the model simulations are able to capture
456 vertical distributions of BC in the SH high latitudes as well as SH and NH mid-latitudes,
457 although the MAM4 simulations with a larger number of mono-layers (e.g., MAM4L8)
458 show too high BC concentrations in the SH high latitudes. The model simulations
459 overestimate BC concentrations in the upper troposphere in all the latitude zones, while
460 they significantly underestimate observed BC concentrations at lower altitudes (below
461 400 hPa) in the NH high latitudes. The low bias of BC concentrations near the surface in
462 the NH high latitudes is improved with MAM4, but there is still an obvious discrepancy
463 between the model simulations and observations. In addition, MAM4 predicts higher BC
464 concentrations than those from MAM3 at all altitudes and all latitude zones in the set 1
465 experiments (Figure 7). With the increase of number of monolayers required for the
466 ageing of primary carbonaceous aerosols in MAM4, modeled BC concentrations increase
467 by up to a factor of 10. The same is true for the higher BC concentrations with MAM4
468 than MAM3 for the set 2 experiments at most altitudes (Figure 8). However, modeled BC
469 concentrations from MAM3 at 1° are higher than those from MAM4 at 2° in the upper
470 troposphere and lower stratosphere. Modeled BC concentrations increase substantially at
471 these altitudes from 2° to 1°. However, the changes are much smaller from 1° to 0.25° at
472 all altitudes for all latitude zones.

473 Figures 9 and 10 compare observed BC vertical profiles from four aircraft
474 campaigns in the tropics (CR-AVE and TC4), NH subtropics (AVE-Houston) and NH
475 mid-latitudes (CARB) with simulations from the set 1 and set 2 experiments,

476 respectively. AVE-Houston, CR-AVE, and TC4 are documented in Schwarz et al. (2006)
477 and CARB is documented in Clarke et al. (2007), Howell et al. (2006), and McNaughton
478 et al. (2009). Observed BC mean concentrations show a strong reduction from the
479 boundary layer to the free troposphere in the tropics (CR-AVE and TC4) and in the
480 subtropics (AVE-Houston), while there is less vertical variation of BC concentrations in
481 the upper troposphere. For the AVE-Houston, CR-AVE, and TC4 campaigns, the model
482 experiments with different numbers of monolayers required for ageing of primary
483 carbonaceous aerosols overestimate BC concentrations in the mid- and upper troposphere
484 (Figure 9), but compare better with observations in the lower troposphere. The CARB
485 campaign in the mid-latitudes of North America in June encountered biomass burning
486 plumes, and elevated BC concentrations were observed at ~800 hPa, which are not
487 captured by model simulations using the AR5 emission inventory. The SD simulations at
488 higher resolutions in the set 2 experiments (Figure 10) do not improve the overall
489 agreement with observations, which indicates the necessity of improving the model
490 physics (e.g., aerosol processing in convective clouds) and aerosol emissions (e.g., for
491 biomass burning aerosols). The modeled BC concentrations do not change significantly
492 with different model resolutions, although there is an increasing trend with increasing the
493 resolution.

494 Figures 11 and 12 compare observed BC vertical profiles from two aircraft
495 campaigns in the NH high latitudes, ARCTAS (Jacob et al., 2010) and ARCPAC (Brock
496 et al., 2011) with the set 1 and set 2 experiments, respectively. Observed BC
497 concentrations show less vertical variations from the surface to ~300 hPa than those in
498 the tropics and NH mid-latitudes, especially in the spring. This results from the poleward

499 transport of BC from NH mid-latitudes at high altitudes. Model simulations in the set 1
500 experiments underestimate observed BC concentrations below altitudes of ~300-400 hPa
501 by 1-2 orders of magnitude, especially in spring (Figure 11). Introducing the primary
502 carbon mode with the number of monolayers increasing from 1 to 8 substantially
503 increases the modeled BC concentrations in the spring, in much better agreement with
504 observations. However, the improvement of BC simulation in the summer is less
505 substantial. The difference of BC concentrations between MAM3 and MAM4 and among
506 different MAM4 experiments is much smaller in the summer, similar in magnitude to the
507 changes in the tropics and NH mid-latitudes (Figure 9). Model simulations in the set 2
508 experiments show the increase of BC concentrations with MAM4, compared to MAM3,
509 but the increase of model resolution does not produce a significant increase of BC
510 concentrations at altitudes below ~200 hPa (Figure 12).

511 Figures 13 and 14 show the seasonal variations of observed BC surface
512 concentrations at four polar sites, in comparison with the model results from MAM4 set 1
513 and 2 experiments, respectively, along with the results from MAM3. Observed BC
514 concentrations at the three Arctic sites show a strong seasonality with higher
515 concentrations in boreal spring and winter, and much lower concentrations in boreal
516 summer (by about one order of magnitude). Observed BC concentrations at the Antarctic
517 site are lower by one order of magnitude than those in the Arctic, and the seasonality is
518 weaker and different, with highest BC concentrations in the austral spring and summer.
519 At the Arctic sites, CAM5 with MAM3 substantially underestimates the observed BC
520 concentrations, especially in winter by more than two orders of magnitude, and produces
521 an opposite seasonality to the observed one. This indicates the too efficient wet

522 scavenging of BC during its transport from the mid-latitudes, especially in spring and
523 winter, since uncertainty of the emissions cannot explain these large discrepancies.
524 CAM5-MAM4, especially with the larger number of monolayers significantly increases
525 the BC concentrations at the Arctic sites, especially in winter, and thus improves the
526 modeled seasonality of BC concentrations. Simulated BC concentrations also increase at
527 the Antarctic site, but the seasonality is still wrong. Increasing the model resolution of
528 CAM5-MAM4 results in a general increase of BC concentrations in different seasons,
529 especially in summer at the Arctic sites, which, however, weakens the simulated
530 seasonality.

531

532 **5. Discussion and conclusions**

533 To reduce the biases of carbonaceous aerosol simulated in CAM5, a new 4-mode
534 version of MAM (MAM4) has been developed by adding a primary carbon mode to the
535 default 3-mode version (MAM3), and by explicitly treating the microphysical ageing of
536 primary carbonaceous aerosols from the primary carbon mode to the accumulation mode.
537 The computational time increases slightly by 10%, comparing to CAM5 with MAM3. As
538 expected, CAM5-MAM4 increases BC and POM burdens and enhances BC transport to
539 remote regions (e.g., Arctic) due to the reduced wet scavenging of BC with more BC
540 residing in the primary carbon mode. The increases are stronger with increasing number
541 of hygroscopic monolayers required for the ageing of primary carbonaceous aerosols.
542 The global burdens of BC and POM increase from 0.087 to 0.123 Tg and from 0.63 to
543 0.96 Tg, respectively, as the number of ageing monolayers is increased from 1 to 8. The
544 BC and POM burdens increase by a factor of 2-10 in the polar regions, depending on the

545 number of monolayers. The global mean lifetimes of BC and POM increase from 4.10 to
546 5.79 days and from 4.62 to 7.02 days, respectively. MAM4 also predicts very similar BC
547 and POM results as MAM7 (Figures not shown).

548 We also explored the sensitivity of modeled carbonaceous aerosol to the
549 horizontal resolution of CAM5-MAM4, as previous studies suggested its importance for
550 the BC transport to remote regions (Ma et al., 2014). The global burdens of BC and POM
551 increase from 0.098 to 0.110 Tg and from 0.81 to 0.87 Tg, respectively, as the resolution
552 increases from 2° to 0.25°. The lifetimes of BC and POM increase from 4.61 to 5.18 days
553 and from 5.91 to 6.35 days, respectively. The largest relative increases in BC and POM
554 burdens occur in the Antarctic, the Arctic, the western and eastern Pacific, and in the East
555 Asian and North American pollution outflows. The increased resolution enhances the
556 transport of aerosols by better resolving mesoscale eddies and the separation of aerosol
557 plumes from clouds and precipitation (Ma et al., 2014).

558 Modeled BC was compared to observations obtained from aircraft campaigns and
559 at polar surface sites. For the vertical profiles of BC concentrations, CAM5-MAM4
560 increases the BC concentrations at all altitudes compared to MAM3. Therefore, MAM4
561 improves the modeled BC in the lower troposphere, especially in the Arctic. The modeled
562 near-surface BC concentrations at the Arctic sites have stronger increases in boreal winter
563 and spring than in summer, which improves the modeled seasonal variation of BC
564 concentrations. However, modeled near-surface BC concentrations in the polar regions
565 are still lower by one order of magnitude compared to observations, even with the
566 number of monolayers of 8 and with the model resolution of 0.25°. This points to the
567 potential problems of emissions and/or other model processes besides the ageing of

568 primary carbonaceous aerosols discussed in this study. H. Wang et al. (2013) found that
569 the wet scavenging of BC might be too efficient in CAM5 due to too high liquid cloud
570 fraction in the NH high latitudes, based on comparison of CAM5 wet scavenging rates
571 with those from the multi-scale modeling framework (MMF) (M. Wang et al., 2011). By
572 modifying the treatment of liquid cloud fraction used in the aerosol activation
573 parameterization, H. Wang et al. (2013) achieved a much better simulation of near-
574 surface BC and other aerosol species in the Arctic compared to the standard CAM5. In
575 addition, the aerosol emission inventories used in our simulations also likely contribute to
576 the BC low biases in the Arctic. They neglect gas flaring emissions in and around the
577 Arctic (Stohl et al., 2013), and they may underestimate fossil fuel emissions in East Asia
578 (Cohen and Wang, 2014).

579 While the modeled BC low bias in the lower troposphere is significantly reduced
580 in the Arctic, the overestimation of BC concentrations in the mid- and upper troposphere
581 over the Pacific and in the tropics and subtropics of North America is exacerbated with
582 MAM4, based on the comparisons with several aircraft campaigns. With a unified
583 treatment of vertical transport and in-cloud wet removal in convective clouds in CAM5,
584 H. Wang et al. (2013) significantly reduced the biases of aerosol distributions in the
585 remote free troposphere predicted by CAM5, due to the inclusion of secondary activation
586 and thus more efficient scavenging of aerosols in convective clouds. An ongoing joint
587 effort between PNNL and NCAR is underway to merge the MAM4 with this unified
588 treatment of convective transport and scavenging. A more recent improved model
589 treatment in the resuspension of aerosols from evaporated raindrops, releasing aerosol
590 particles to the coarse mode instead of their originating mode upon complete evaporation

591 of raindrops (Easter et al., 2015, personal communication), has shown a significant
592 impact on the vertical distribution of aerosols, including large reductions in mid- and
593 upper tropospheric BC and POM. This emphasizes the importance of improving the
594 representations of clouds and precipitation and aerosol-cloud interactions in GCMs.

595 We note that in this study, we only present the results and analysis of primary
596 carbonaceous aerosols, especially BC, since there have been more BC measurements, and
597 POM is co-emitted with BC. The lifecycle and global budgets of other aerosol species
598 such as sulfate, SOA, sea salt and dust are not presented in this study, since introducing
599 the primary carbon mode has a negligible effect on these aerosol species. This is expected
600 since sulfate and SOA primarily reside in the accumulation mode, while dust and sea salt
601 are mostly in the accumulation and coarse modes. Changes in modeled CCN
602 concentrations are also small. The change in the “effective” radiative forcing due to
603 anthropogenic aerosol-radiation and anthropogenic aerosol-cloud interactions induced by
604 the MAM4 implementation is less than 0.1 W m^{-2} in the global mean.

605

606 **Code availability**

607 The release of CESM version 1.2.0 (with CAM5.3) can be obtained at
608 (<http://www.cesm.ucar.edu/models/cesm1.2/>). Code modifications for the 4-mode version
609 of Modal Aerosol Module are available upon request by contacting the corresponding
610 author.

611

612 **Acknowledgments:**

613 This work was supported by the U.S. Department of Energy, Office of Biological and
614 Environmental Research, Earth System Modeling Program. The Pacific Northwest

615 National Laboratory is operated for DOE by Battelle Memorial Institute under contract
616 DE-AC05-76RL01830. The National Center for Atmospheric Research is funded by the
617 National Science Foundation.

618

619 **References**

620

621 Abdul-Razzak, H., and S. J. Ghan (2000), A parameterization of aerosol activation 2.
622 Multiple aerosol types, *J. Geophys. Res.*, *105*, 6837-6844.

623

624 Adachi, K., S. H. Chung, and P. R. Buseck (2010), Shapes of soot aerosol particles and
625 implications for their effects on climate, *J. Geophys. Res.*, *115*, D15206,
626 doi:10.1029/2009JD012868.

627

628 Bauer, S. E., Wright, D. L., Koch, D., Lewis, E. R., McGraw, R., Chang, L.-S.,
629 Schwartz, S. E., and Ruedy, R. (2008), MATRIX (Multiconfiguration Aerosol
630 TRacker of mIXing state): an aerosol microphysical module for global atmospheric
631 models, *Atmos. Chem. Phys.*, *8*, 6003–6035, doi:10.5194/acp-8-6003-2008.

632

633 Bian, H., Colarco, P. R., Chin, M., Chen, G., Rodriguez, J. M., Liang, Q., Blake, D.,
634 Chu, D. A., da Silva, A., Darmenov, A. S., Diskin, G., Fuelberg, H. E., Huey, G.,
635 Kondo, Y., Nielsen, J. E., Pan, X., and Wisthaler, A.: Source attributions of pollution
636 to the Western Arctic during the NASA ARCTAS field campaign, *Atmos. Chem.*
637 *Phys.*, *13*, 4707-4721, doi:10.5194/acp-13-4707-2013, 2013.

638

639 Bond, T. C., S. J. Doherty, D. W. Fahey, P. Forster, T. Berntsen, B. J. DeAngelo, M. G.
640 Flanner, S. J. Ghan, B. Karcher, D. Koch, S. Kinne, Y. Kondo, P. K. Quinn, M.
641 Sarofim, M. Schultz, M. Schulz, C. Venkataraman, H. Zhang, S. Zhang, N. Bellouin,
642 S. K. Guttikunda, P. K. Hopke, M. Z. Jacobson, J. W. Kaiser, Z. Klimont, U.
643 Lohmann, J. P. Schwarz, D. Shindell, T. Storelvmo, S. G. Warren, and C. S.
644 Zender (2013), Bounding the role of black carbon in the climate system: A scientific
645 assessment, *J. Geophys. Res.*, *118*, 5380-5552, doi: 10.1002/jgrd.50171.

646

647 Bretherton, C. S., and S. Park (2009), A new moist turbulence parameterization in the
648 Community Atmosphere Model. *J. Climate*, *22*, 3422–3448.

649

650 Brock, C. A., Cozic, J., Bahreini, R., Froyd, K. D., Middlebrook, A. M.,
651 McComiskey, A., Brioude, J., Cooper, O. R., Stohl, A., Aikin, K. C., de Gouw, J. A.,
652 Fahey, D. W., Ferrare, R. A., Gao, R.-S., Gore, W., Holloway, J. S., Hübler, G.,
653 Jefferson, A., Lack, D. A., Lance, S., Moore, R. H., Murphy, D. M., Nenes, A.,
654 Novelli, P. C., Nowak, J. B., Ogren, J. A., Peischl, J., Pierce, R. B., Pilewskie, P.,
655 Quinn, P. K., Ryerson, T. B., Schmidt, K. S., Schwarz, J. P., Sodemann, H.,
656 Spackman, J. R., Stark, H., Thomson, D. S., Thornberry, T., Veres, P., Watts, L. A.,
657 Warneke, C., and Wollny, A. G.: Characteristics, sources, and transport of aerosols
658 measured in spring 2008 during the aerosol, radiation, and cloud processes affecting
659 Arctic Climate (ARCPAC) Project, *Atmos. Chem. Phys.*, *11*, 2423-2453,
660 doi:10.5194/acp-11-2423-2011, 2011.

661

662 Clarke, A., et al. (2007), Biomass burning and pollution aerosol over North America:
663 Organic components and their influence on spectral optical properties and

664 humidification response, *J. Geophys. Res.*, 112, D12S18,
665 doi:10.1029/2006JD007777.

666

667 Cohen, J. B., and C. Wang (2014), Estimating global black carbon emissions using a top-
668 down Kalman Filter approach, *J. Geophys. Res.*, 119, 307–323,
669 doi:10.1002/2013JD019912.

670

671 Cooke, W. F., and J. J. N. Wilson (1996), A global black carbon aerosol model, *J.*
672 *Geophys. Res.*, 101, 19,395–19,409.

673

674 Flanner, M. G., C. S. Zender, J. T. Randerson, and P. J. Rasch (2007), Present-day
675 climate forcing and response from black carbon in snow, *J. Geophys. Res.*, 112,
676 D11202, doi:1029/2006JD008003.

677

678 Flanner, M. G., C. S. Zender, P. G. Hess, N. M. Mahowald, T. H. Painter, V.
679 Ramanathan, and P. J. Rasch (2009), Springtime warming and reduced snow cover
680 from carbonaceous particles, *Atmos. Chem. Phys.*, 9, 2481–2497, doi:10.5194/acp-9-
681 2481-2009.

682

683 Flanner, M. G., Liu, X., Zhou, C., Penner, J. E., and Jiao, C. (2012), Enhanced solar
684 energy absorption by internally-mixed black carbon in snow grains, *Atmos. Chem.*
685 *Phys.*, 12, 4699-4721, doi:10.5194/acp-12-4699-2012.

686

687 Forster, P., Ramaswamy, V., Artaxo, P., Berntsen, T., Betts, R., Fahey, D. W., Haywood,
688 J., Lean, J., Lowe, D. C., Myhre, G., Nganga, J., Prinn, R., Raga, G., Schulz, M., and
689 Van Dorland, R: Changes in atmospheric constituents and in radiative forcing, in:
690 Climate Change 2007: The Physical Science Basis, Contribution of Working Group I
691 to the Fourth Assessment Report of the Intergovernmental Panel on Climate Change,
692 Cambridge University Press, Cambridge, New York, 129–234, 2007.

693

694 Gao, Y., C. Zhao, X. Liu, M. Zhang, and L.-R. Leung (2014), WRF-Chem simulations of
695 aerosols and anthropogenic aerosol radiative forcing in East Asia, *Atmos. Environ.*,
696 92, 250-266, doi: 10.1016/j.atmosenv.2014.04.038.

697

698 Gettelman, A., X. Liu, S. J. Ghan, H. Morrison, S. Park, A. J. Conley, S. A. Klein, J.
699 Boyle, D. L. Mitchell, and J.-L. F. Li (2010), Global simulations of ice nucleation
700 and ice supersaturation with an improved cloud scheme in the Community
701 Atmosphere Model. *J. Geophys. Res.*, 115, D18216, doi:10.1029/2009JD013797.

702

703 Ghan, S. J., and R. C. Easter (2006), Impact of cloud-borne aerosol representation on
704 aerosol direct and indirect effects. *Atmos. Chem. & Phys.*, 6, 4163–4174. See
705 correction *Atmos. Chem. Phys.*, 7, 293–294, 2007.

706

707 Hansen, J. and L. Nazarenko (2004), Soot climate forcing via snow and ice albedos, *Proc.*
708 *Natl. Acad. Sci. (USA)*, 101, 423–428.

709

710 Hansen, J., Sato, M., Ruedy, R., Nazarenko, L., Lacis, A., Schmidt, G. A., Russell, G.,
711 Aleinov, I., Bauer, M., Bauer, S., Bell, N., Cairns, B., Canuto, V., Chandler, M.,
712 Cheng, Y., Genio, A. D., Faluvegi, G., Fleming, E., Friend, A., Hall, T., Jackman,
713 C., Kelley, M., Kiang, N., Koch, D., Lean, J., Lerner, J., Lo, K., Menon, S., Miller,
714 R., Minnis, P., Novakov, T., Oinas, V., Perlwitz, J., Perlwitz, J., Rind, D., Romanou,
715 A., Shindell, D., Stone, P., Sun, S., Tausnev, N., Thresher, D., Wielicki, B., Wong,
716 T., Yao, M., and Zhang, S. (2005), Efficacy of climate forcings, *J. Geophys. Res.*,
717 *110*, D18104, doi:10.1029/2005JD005776.

718

719 Howell, S. G., A. D. Clarke, Y. Shinozuka, V. Kapustin, C. S. McNaughton, B. J.
720 Huebert, S. J. Doherty, and T. L. Anderson (2006), Influence of relative humidity
721 upon pollution and dust during ACE-Asia: Size distributions and implications for
722 optical properties, *J. Geophys. Res.*, *111*, D06205, doi:10.1029/2004JD005759.

723

724 Iacono, M. J., J. S. Delamere, E. J. Mlawer, M. W. Shephard, S. A. Clough and W. D.
725 Collins (2008), Radiative forcing by long-lived greenhouse gases: Calculations with
726 the AER radiative transfer models. *J. Geophys. Res.*, *113*, D13103, doi:
727 10.1029/2008jd009944.

728

729 Jacob, D. J., Crawford, J. H., Maring, H., Clarke, A. D., Dibb, J. E., Emmons, L. K.,
730 Ferrare, R. A., Hostetler, C. A., Russell, P. B., Singh, H. B., Thompson, A. M.,
731 Shaw, G. E., McCauley, E., Pederson, J. R., and Fisher, J. A.: The Arctic Research of
732 the Composition of the Troposphere from Aircraft and Satellites (ARCTAS)
733 mission: design, execution, and first results, *Atmos. Chem. Phys.*, *10*, 5191-5212,
734 doi:10.5194/acp-10-5191-2010, 2010.

735

736 Jacobson, M. Z. (2001), Strong radiative heating due to the mixing state of black carbon
737 in atmospheric aerosols, *Nature*, *409*, 695-697.

738

739 Jacobson, M. Z. (2003), Reply to comment by J. Feichter et al. on “Control of fossil-fuel
740 particulate black carbon and organic matter, possibly the most effective method of
741 slowing global warming”, *J. Geophys. Res.*, *108*, 4768, doi:10.1029/2002JD003299.

742

743 Jacobson, M. Z. (2004), Climate response of fossil fuel and biofuel soot, accounting for
744 soot’s feedback to snow and sea ice albedo and emissivity, *J. Geophys. Res.*, *109*,
745 D21201, doi:10.1029/2004JD004945.

746

747 Jiao, C., Flanner, M. G., Balkanski, Y., Bauer, S. E., Bellouin, N., Berntsen, T. K.,
748 Bian, H., Carslaw, K. S., Chin, M., De Luca, N., Diehl, T., Ghan, S. J., Iversen, T.,
749 Kirkevåg, A., Koch, D., Liu, X., Mann, G. W., Penner, J. E., Pitari, G., Schulz, M.,
750 Seland, Ø., Skeie, R. B., Steenrod, S. D., Stier, P., Takemura, T., Tsigaridis, K.,
751 van Noije, T., Yun, Y., and Zhang, K.: An AeroCom assessment of black carbon in
752 Arctic snow and sea ice, *Atmos. Chem. Phys.*, *14*, 2399-2417, doi:10.5194/acp-14-
753 2399-2014, 2014.

754

755 Kinne, S., M. Schulz, C. Textor et al. (2006), An AeroCom initial assessment – optical

756 properties in aerosol component modules of global models, *Atmos. Chem. Phys.*, *6*,
757 1815–1834.
758

759 Kipling, Z., Stier, P., Schwarz, J. P., Perring, A. E., Spackman, J. R., Mann, G. W.,
760 Johnson, C. E., and Telford, P. J.: Constraints on aerosol processes in climate models
761 from vertically-resolved aircraft observations of black carbon, *Atmos. Chem. Phys.*,
762 *13*, 5969–5986, doi:10.5194/acp-13-5969-2013, 2013.
763

764 Koch, D., et al. (2009), Evaluation of black carbon estimations in global aerosol models,
765 *Atmos. Chem. Phys.*, *9*, 9001–9026.
766

767 Lamarque, J. F., et al. (2010), Historical (1850–2000) gridded anthropogenic and biomass
768 burning emissions of reactive gases and aerosols: methodology and application,
769 *Atmos. Chem. Phys.*, *10*, 7017–7039.
770

771 Liu, J., Fan, S., Horowitz, L. W., and Levy, H.: Evaluation of factors controlling long-
772 range transport of black carbon to the Arctic, *J. Geophys. Res.*, *116*, D04307,
773 doi:10.1029/2010JD015145, 2011.
774

775 Liu, X., and J. E. Penner (2005), Ice nucleation parameterization for global models,
776 *Meteorologische Zeitschrift*, *14*, 499-514.
777

778 Liu, X., and J. Wang (2010), How important is organic aerosol hygroscopicity to aerosol
779 indirect forcing? *Environ. Res. Lett.*, *5*, 044010, doi: 10.1088/1748-9326/5/4/044010.
780

781 Liu, X., J. E. Penner, and M. Herzog (2005), Global simulation of aerosol dynamics:
782 Model description, evaluation, and interactions between sulfate and nonsulfate
783 aerosols, *J. Geophys. Res.*, *110*, No. D18, D18206, doi:10.1029/2004JD005674.
784

785 Liu, X., J. E. Penner, S. J. Ghan, and M. Wang (2007), Inclusion of ice microphysics in
786 the NCAR Community Atmospheric Model version 3 (CAM3), *J. Climate*, *20*, 4526-
787 4547.
788

789 Liu, X., R. C. Easter, S. J. Ghan, R. Zaveri, P. Rasch, X. Shi, J. F. Lamarque, A.
790 Gettelman, H. Morrison, F. Vitt, A. Conley, S. Park, R. Neale, C. Hannay, A. M. L.
791 Ekman, P. Hess, N. Mahowald, W. Collins, M. J. Iacono, C. S. Bretherton, M. G.
792 Flanner, and D. Mitchell (2012), Toward a minimal representation of aerosols in
793 climate models: description and evaluation in the Community Atmosphere Model
794 CAM5, *Geosci. Model Dev.*, *5*, 709-739.
795

796 Ma, P.-L., P. J. Rasch, H. Wang, K. Zhang, R. C. Easter, S. Tilmes, J. D. Fast, X. Liu, J.-
797 H. Yoon, and J.-F. Lamarque (2013a), The role of circulation features on black
798 carbon transport into the Arctic in the Community Atmosphere Model version 5
799 (CAM5), *J. Geophys. Res.*, *118*, 4657–4669, doi:10.1002/jgrd.50411.
800

801 Ma, P.-L., J. R. Gattiker, X. Liu, and P. J. Rasch (2013b), A novel approach for
802 determining source–receptor relationships in model simulations: a case study of
803 black carbon transport in northern hemisphere winter, *Environ. Res. Lett.*, *8*, 024042,
804 doi:10.1088/1748-9326/8/2/024042.

805

806 Ma, P.-L., P. J. Rasch, J. D. Fast, R. C. Easter, W. I. Gustafson Jr., X. Liu, S. J. Ghan,
807 and B. Singh (2014), Assessing the CAM5 physics suite in the WRF-Chem model:
808 Implementation, resolution sensitivity, and a first evaluation for a regional case study,
809 *Geosci. Model Dev.*, *7*, 755–778, doi:10.5194/gmd-7-755-2014.

810

811 Ma, P.-L., P. J. Rasch, M. Wang, H. Wang, S. J. Ghan, R. C. Easter, W. I. Gustafson Jr.,
812 X. Liu, Y. Zhang, and H.-Y. Ma (2015), How does increasing horizontal resolution
813 in a global climate model improve the simulation of aerosol-cloud interactions?,
814 *Geophys. Res. Lett.*, *42*, 5058–5065, doi:10.1002/2015GL064183.

815

816 McNaughton, C. S., Clarke, A. D., Kapustin, V., Shinozuka, Y., Howell, S. G.,
817 Anderson, B. E., Winstead, E., Dibb, J., Scheuer, E., Cohen, R. C., Wooldridge, P.,
818 Perring, A., Huey, L. G., Kim, S., Jimenez, J. L., Dunlea, E. J., DeCarlo, P. F.,
819 Wennberg, P. O., Crounse, J. D., Weinheimer, A. J., and Flocke, F.: Observations of
820 heterogeneous reactions between Asian pollution and mineral dust over the Eastern
821 North Pacific during INTEX-B, *Atmos. Chem. Phys.*, *9*, 8283-8308, doi:10.5194/acp-
822 9-8283-2009, 2009.

823

824 Morrison, H., and A. Gettelman (2008), A new two-moment bulk stratiform cloud
825 microphysics scheme in the community atmosphere model, version 3 (CAM3). Part
826 I: Description and numerical tests, *J. Climate*, *21*(15): 3642-3659, doi:
827 10.1175/2008jcli2105.1.

828

829 Myhre, G., Shindell, D., Bréon, F.-M., Collins, W., Fuglestedt, J., Huang, J., Koch, D.,
830 Lamarque, J.-F., Lee, D., Mendoza, B., Nakajima, T., Robock, A., Stephens, G.,
831 Takemura, T., and Zhang, H.: Anthropogenic and natural radiative forcing, in:
832 *Climate Change 2013: The Physical Science Basis, Contribution of Working Group I*
833 *to the Fifth Assessment Report of the Intergovernmental Panel on Climate Change*,
834 Cambridge University Press, Cambridge, UK, New York, NY, USA, 659–740, 2013.

835

836 Neale, R. B., J. H. Richter, and M. Jochum (2008), The impact of convection on ENSO:
837 From a delayed oscillator to a series of events, *J. Climate*, *21*(22): 5904-5924, doi:
838 10.1175/2008jcli2244.1.

839

840 Neale, R. B., Chen, C.-C., Gettelman, A., Lauritzen, P. H., Park, S., Williamson, D. L.,
841 Conley, A. J., Garcia, R., Kinnison, D., Lamarque, J.-F., Marsh, D., Mills, M.,
842 Smith, A. K., Tilmes, S., Vitt, F., Cameron-Smith, P., Collins, W. D., Iacono, M. J.,
843 Easter, R. C., Ghan, S. J., Liu, X., Rasch, P. J., and Taylor, M. A.: Description of the
844 NCAR Community Atmosphere Model (CAM 5.0), NCAR/TN-486+ STR, available
845 at: http://www.cesm.ucar.edu/models/cesm1.0/cam/docs/description/cam5_desc.pdf,
846 2012.

847
848 Park, S. and C. S. Bretherton (2009), The University of Washington Shallow Convection
849 and Moist Turbulence Schemes and Their Impact on Climate Simulations with the
850 Community Atmosphere Model, *J. Climate*, 22(12): 3449-3469, doi:
851 10.1175/2008jcli2557.1.
852
853 Park, S., C. S. Bretherton, and P. J. Rasch (2014), Integrating cloud processes in the
854 Community Atmosphere Model, Version 5, *J. Climate*, 27, 6821-6856. doi:
855 10.1175/JCLI-D-14-00087.1.
856
857 Quaas, J., Ming, Y., Menon, S., Takemura, T., Wang, M., Penner, J. E., Gettelman, A.,
858 Lohmann, U., Bellouin, N., Boucher, O., Sayer, A. M., Thomas, G. E., McComiskey,
859 A., Feingold, G., Hoose, C., Kristjánsson, J. E., Liu, X., Balkanski, Y., Donner, L. J.,
860 Ginoux, P. A., Stier, P., Grandey, B., Feichter, J., Sednev, I., Bauer, S. E., Koch, D.,
861 Grainger, R. G., Kirkevåg, A., Iversen, T., Seland, Ø., Easter, R., Ghan, S. J., Rasch,
862 P. J., Morrison, H., Lamarque, J.-F., Iacono, M. J., Kinne, S., and Schulz, M.:
863 Aerosol indirect effects – general circulation model intercomparison and evaluation
864 with satellite data, *Atmos. Chem. Phys.*, 9, 8697–8717, doi:10.5194/acp-9-8697-
865 2009, 2009.
866
867 Richter, J. H. and P. J. Rasch (2008), Effects of convective momentum transport on the
868 atmospheric circulation in the community atmosphere model, version 3, *J. Climate*,
869 21, 1487-1499. doi: 10.1175/2007jcli1789.1.
870
871 Riemer, N., M. West, R. A. Zaveri, and R. C. Easter (2009), Simulating the evolution of
872 soot mixing state with a particle-resolved aerosol model, *J. Geophys. Res.*, 114,
873 D09202, doi:10.1029/2008JD011073.
874
875 Samset, B. H., Myhre, G., Herber, A., Kondo, Y., Li, S.-M., Moteki, N., Koike, M.,
876 Oshima, N., Schwarz, J. P., Balkanski, Y., Bauer, S. E., Bellouin, N.,
877 Berntsen, T. K., Bian, H., Chin, M., Diehl, T., Easter, R. C., Ghan, S. J., Iversen, T.,
878 Kirkevåg, A., Lamarque, J.-F., Lin, G., Liu, X., Penner, J. E., Schulz, M., Seland, Ø.,
879 Skeie, R. B., Stier, P., Takemura, T., Tsigaridis, K., and Zhang, K.: Modelled black
880 carbon radiative forcing and atmospheric lifetime in AeroCom Phase II constrained
881 by aircraft observations, *Atmos. Chem. Phys.*, 14, 12465-12477, doi:10.5194/acp-14-
882 12465-2014, 2014.
883
884 Schwarz, J. P., et al. (2006), Single-particle measurements of midlatitude black carbon
885 and light-scattering aerosols from the boundary layer to the lower stratosphere, *J.*
886 *Geophys. Res.*, 111, D16207, doi:10.1029/2006JD007076.
887
888 Schwarz, J. P., J. R. Spackman, R. S. Gao, L. A. Watts, P. Stier, M. Schulz, S. M. Davis,
889 S. C. Wofsy, and D. W. Fahey (2010), Global-scale black carbon profiles observed
890 in the remote atmosphere and compared to models, *Geophys. Res. Lett.*, 37, L18812,
891 doi:10.1029/2010GL044372.
892

893 Schwarz, J. P., B. H. Samset, A. E. Perring, J. R. Spackman, R. S. Gao, P. Stier, M.
894 Schulz, F. L. Moore, E. A. Ray, and D. W. Fahey (2013), Global-scale seasonally
895 resolved black carbon vertical profiles over the Pacific, *Geophys. Res. Lett.*, *40*,
896 5542–5547, doi:10.1002/2013GL057775.

897
898 Spracklen, D. V., Pringle, K. J., Carslaw, K. S., Chipperfield, M. P., and Mann, G. W.
899 (2005), A global off-line model of size-resolved aerosol microphysics: I. Model
900 development and prediction of aerosol properties, *Atmos. Chem. Phys.*, *5*, 2227–
901 2252, doi:10.5194/acp-5-2227-2005.

902
903 Stier, P., Feichter, J., Kinne, S., Kloster, S., Vignati, E., Wilson, J., Ganzeveld, L., Tegen,
904 I., Werner, M., Balkanski, Y., Schulz, M., Boucher, O., Minikin, A., and Petzold, A.
905 (2005), The aerosol-climate model ECHAM5-HAM, *Atmos. Chem. Phys.*, *5*, 1125–
906 1156, doi:10.5194/acp-5-1125-2005.

907
908 Stohl, A., Z. Klimont, S. Eckhardt, K. Kupiainen, V. P. Shevchenko, V. M. Kopeikin,
909 and A. N. Novigatsky (2013), Black carbon in the Arctic: The underestimated role of
910 gas flaring and residential combustion emissions, *Atmos. Chem. Phys.*, *13*, 8833–
911 8855, doi:10.5194/acp-13-8833-2013.

912
913 Schulz, M., C. Textor, S. Kinne, Y. Balkanski, S. Bauer, T. Berntse, T. Berglen, O.
914 Boucher, F. Dentener, S. Guibert, I.S.A. Isaksen, T. Iversen, D. Koch, A. Kirkevåg,
915 X. Liu, V. Montanaro, G. Myhre, J. Penner, G. Pitari, S. Reddy, O. Seland, P. Stier,
916 and T. Takemura (2006), Radiative forcing by aerosols as derived from the
917 AeroCom present-day and pre-industrial simulations, *Atmos. Chem. Phys.*, *6*, 5225–
918 5246.

919
920 Textor, C., M. Schulz, S. Guibert, S. Kinne, Y. Balkanski, S. Bauer, T. Berntsen, T.
921 Berglen, O. Boucher, M. Chin, F. Dentener, T. Diehl, R. Easter, H. Feichter, D.
922 Fillmore, S. Ghan, P. Ginoux, S. Gong, A. Grini, J. Hendricks, L. Horowitz, P.
923 Huang, I. Isaksen, T. Iversen, S. Kloster, D. Koch, A. Kirkevåg, J.E. Kristjansson, M.
924 Krol, A. Lauer, J.F. Lamarque, X. Liu, V. Montanaro, G. Myhre, J. Penner, G. Pitari,
925 S. Reddy, Ø. Seland, P. Stier, T. Takemura, and X. Tie (2006), Analysis and
926 quantification of the diversities of aerosol life cycles within AeroCom, *Atmos. Chem.*
927 *Phys.*, *6*, 1777-1813.

928
929 Tie, X., S. Madronich, S. Walters, D. P. Edwards, P. Ginoux, N. Mahowald, R. Zhang, C.
930 Lou, and G. Brasseur (2005), Assessment of the global impact of aerosols on
931 tropospheric oxidants, *J. Geophys. Res.*, *110*, D03204, doi:10.1029/2004JD005359.

932
933 Tilmes, S., J.-F. Lamarque, L. K. Emmons, D. E. Kinnison, P. L. Ma, X. Liu, S. Ghan, C.
934 Bardeen, S. Arnold, M. Deeter, F. Vitt, T. Ryerson, J. W. Elkins, F. Moore, R.
935 Spackman, and M. Val Martin (2015), Description and evaluation of
936 tropospheric chemistry and aerosols in the Community Earth System Model
937 (CESM1.2), *Geosci. Model Dev.*, *8*, 1395–1426, doi:10.5194/gmd-8-1395-2015.

938

939 Wang, M., S. J. Ghan, R. C. Easter, M. Ovchinnikov, X. Liu, E. Kassianov, Y. Qian, W.
940 Gustafson, V. E. Larson, D. P. Schanen, M. Khairoutdinov, and H. Morrison (2011),
941 The multi-scale aerosol-climate model PNNL-MMF: model description and
942 evaluations, *Geosci. Model Dev.*, *4*, 137-168.
943
944 Wang, H., R. C. Easter, P. J. Rasch, M. Wang, X. Liu, S. J. Ghan, Y. Qian, J.-H. Yoon,
945 P.-L. Ma, and V. Velu (2013), Improving aerosol transport to high-latitudes in
946 CAM5, *Geosci. Model Dev.*, *6*, 765–782, doi:10.5194/gmd-6-765-2013.
947
948 Wofsy, S. C. and the HIPPO team: HIAPER Pole-to-Pole Observations (HIPPO): fine-
949 grained, global-scale measurements of climatically important atmospheric gases and
950 aerosols, *Philos. T. Ser. A*, *369*, 2073–86, doi:10.1098/rsta.2010.0313, 2011.
951
952 Zhang, G. J. and N. A. McFarlane (1995), Sensitivity of Climate Simulations to the
953 Parameterization of Cumulus Convection in the Canadian Climate Center General-
954 Circulation Model, *Atmosphere-Ocean*, *33*(3): 407-446.
955
956 Zhang, K., H. Wan, X. Liu, S. Ghan, G. J. Kooperman, P.-L. Ma, and P. J. Rasch, D.
957 Neubauer, and U. Lohmann (2014), Technical Note: On the use of nudging for
958 aerosol-climate model intercomparison studies, *Atmos. Chem. Phys.*, *14*, 8631–8645,
959 doi:10.5194/acp-14-8631-2014.
960

961 **Table Captions**

962

963 Table 1. Model experiments. Set 1 experiments are to test the model sensitivity to the
964 criterion of number of ageing monolayers, running CAM5-MAM4 in free-running
965 simulations at horizontal resolution of 1°. Set 2 experiments are to test the model
966 sensitivity to the model horizontal resolution, running CAM5-MAM4 in specified
967 dynamics (SD) simulations with the number of ageing monolayers set to 8. In both sets of
968 experiments the standard CAM5.3 with MAM3 is run for the comparison.

969

970 Table 2. Global BC budgets for monolayer sensitivity simulations in set 1 experiments.
971 Numbers in parentheses are standard deviations about the 10-year mean representing
972 inter-annual variability.

973

974 Table 3. Same as Table 2, except for POM budgets.

975

976 Table 4. Global BC budgets for resolution sensitivity simulations in set 2 experiments.

977

978 Table 5. Same as Table 4, except for POM budgets.

979

980 **Figure Captions**

981

982 Figure 1. Schematic of aerosol modes and associated aerosol tracers in MAM4.

983

984 Figure 2. Latitudinal and longitudinal distributions of annual mean column burdens of
985 BC (in $10^2 \mu\text{g m}^{-2}$, left) and POM ($10^3 \mu\text{g m}^{-2}$, right) from the set 1 experiments with the
986 default MAM3, and MAM4 with different criteria of number of monolayers (i.e.,
987 MAM4L1, MAM4L2, MAM4L4, and MAM4L8).

988

989 Figure 3. Latitudinal and longitudinal distributions of the relative (percentage)
990 differences of annual mean burdens of BC (left) and POM (right) between MAM4 with
991 different criteria of number of monolayers (i.e., MAM4L1, MAM4L2, MAM4L4, and
992 MAM4L8) and MAM3 in the set 1 experiments.

993

994 Figure 4. Latitudinal and longitudinal distributions of annual mean column burdens of
995 BC (in $10^2 \mu\text{g m}^{-2}$, left) and POM ($10^3 \mu\text{g m}^{-2}$, right) from the set 2 experiments with the
996 default MAM3 at 1° horizontal resolution (MAM3R1), and MAM4 at different horizontal
997 resolutions (i.e., MAM4R2, MAM4R1, MAM4R0.5, and MAM4R0.25).

998

999 Figure 5. Latitudinal and longitudinal distributions of the relative (percentage)
1000 differences of annual mean burdens of BC (left) and POM (right) from the set 2
1001 experiments with MAM4 at 1° , 0.5° , and 0.25° relative to 2° horizontal resolution.

1002

1003 Figure 6. Latitude and altitude cross section of observed and simulated BC concentrations
1004 (in ng m^{-3}) during the HIAPER (High-Performance Instrumented Airborne Platform for
1005 Environmental Research) Pole-to-Pole Observations (HIPPO) campaigns (HIPPO 1-5)
1006 over the remote Pacific from 80°N to 67°S in January and November 2009, March/April
1007 2010, and June/July and August/September 2011. MAM4 simulated BC concentrations
1008 for the same time periods in the set 2 experiments at different horizontal resolutions (i.e.,
1009 MAM4R2, MAM4R1, MAM4R0.5, and MAM4R0.25) are used for comparison. The
1010 model simulations are sampled along the flight paths.

1011

1012 Figure 7. Observed and simulated vertical profiles of BC concentrations (in ng kg^{-1})
1013 during the HIPPO1 campaign over the Arctic and remote Pacific in January 2009. Dark
1014 solid curves are for observation means, and shaded areas for the plus/minus one standard
1015 deviation of observations. The CAM5 simulations in the set 1 experiments (i.e., MAM3,
1016 MAM4L1, MAM4L2, MAM4L4, and MAM4L8) are used for comparison. Simulated
1017 profiles are averaged over the points on the map and the indicated month of the field
1018 campaign.

1019

1020 Figure 8. Same as Figure 7, except for CAM5 simulations in the set 2 experiments (i.e.,
1021 MAM3R1, MAM4R2, MAM4R1, MAM4R0.5, and MAM4R0.25).

1022

1023 Figure 9. Observed and simulated vertical profiles of BC concentrations (in ng kg^{-1}) from
1024 four aircraft campaigns in the tropics, NH subtropics and NH mid-latitudes: AVE-
1025 Houston (NASA Houston Aura Validation Experiment) in November 2010 and 2012,

1026 respectively, CR-AVE (NASA Costa Rica Aura Validation Experiment) in February
1027 2006, TC4 (Tropical Composition, Cloud and Climate Coupling) in August 2007, and
1028 CARB (NASA initiative in collaboration with California Air Resources Board) in June
1029 2008. Observations are averages for the respective campaigns with dark solid curves for
1030 observation means, dark dashed curves for observation medians, and shaded areas for the
1031 plus/minus one standard deviation of observations. Simulated profiles for the CAM5
1032 simulations in the set 1 experiments (i.e., MAM3, MAM4L1, MAM4L2, MAM4L4, and
1033 MAM4L8) are averaged over the points on the map and the indicated month of respective
1034 field campaign.

1035
1036 Figure 10. Same as Figure 9, except for CAM5 simulations in the set 2 experiments (i.e.,
1037 MAM3R1, MAM4R2, MAM4R1, MAM4R0.5, and MAM4R0.25).

1038
1039 Figure 11. Same as Figure 9, except for BC profiles in the NH high latitudes from two
1040 other aircraft campaigns: ARCTAS (NASA Arctic Research of the Composition of the
1041 Troposphere from Aircraft and Satellite) in spring (April) and summer (June-July) 2008,
1042 and ARCPAC (NOAA Aerosol, Radiation, and Cloud Processes affecting Arctic
1043 Climate) in spring (April) 2008. Simulated profiles are averaged over the points on the
1044 map and the indicated month of respective field campaign.

1045
1046 Figure 12. Same as Figure 11, except for CAM5 simulations in the set 2 experiments.

1047
1048 Figure 13. Seasonal variations of observed and simulated BC surface concentrations (in
1049 ng kg^{-1}) at four polar sites. CAM5 simulations in the set 1 experiments (i.e., MAM3,
1050 MAM4L1, MAM4L2, MAM4L4, and MAM4L8) are used for comparison.

1051
1052 Figure 14. Same as Figure 13, except for CAM5 simulations in the set 2 experiments (i.e.,
1053 MAM3R1, MAM4R2, MAM4R1, MAM4R0.5, and MAM4R0.25).

1054

1055 Table 1. Model experiments. Set 1 experiments are to test the model sensitivity to the
 1056 criterion of number of ageing monolayers, running CAM5-MAM4 in free-running
 1057 simulations at horizontal resolution of 1°. Set 2 experiments are to test the model
 1058 sensitivity to the model horizontal resolution, running CAM5-MAM4 in specified
 1059 dynamics (SD) simulations with the number of ageing monolayers set to 8. In both sets of
 1060 experiments the standard CAM5.3 with MAM3 is run for the comparison.
 1061

Experiment Name	Mono-layer	Horizontal Resolution	Simulation Type	
Set 1	MAM4L1	1	1°	Free-running
	MAM4L2	2	1°	Free-running
	MAM4L4	4	1°	Free-running
	MAM4L8	8	1°	Free-running
	MAM3	N/A	1°	Free-running
Set 2	MAM4R2	8	2°	SD
	MAM4R1	8	1°	SD
	MAM4R0.5	8	0.5°	SD
	MAM4R0.25	8	0.25°	SD
	MAM3R1	N/A	1°	SD

1062

1063

1064

1065 Table 2. Global BC budgets for monolayer sensitivity simulations in set 1 experiments.

1066 Numbers in parentheses are standard deviations about the 10-year mean representing

1067 inter-annual variability.

1068

	MAM3	MAM4L1	MAM4L2	MAM4L4	MAM4L8
Sources (Tg/yr)	7.76	7.76	7.76	7.76	7.76
Emission	7.76	7.76	7.76	7.76	7.76
Sinks (Tg/yr)	7.75 (0.008)	7.75 (0.004)	7.75 (0.007)	7.75 (0.006)	7.74 (0.006)
Dry deposition	1.30 (0.014)	1.38 (0.006)	1.42 (0.013)	1.50 (0.009)	1.64 (0.009)
Wet deposition	6.45 (0.014)	6.37 (0.008)	6.33 (0.015)	6.25 (0.011)	6.10 (0.006)
Lifetime (days)	3.95 (0.048)	4.10 (0.036)	4.30 (0.037)	4.80 (0.031)	5.79 (0.051)
Burden (Tg)	0.084 (0.001)	0.087 (0.008)	0.091 (0.0007)	0.102 (0.0007)	0.123 (0.001)
in accumulation	0.084 (0.001)	0.082 (0.007)	0.082 (0.0008)	0.083 (0.0007)	0.083 (0.001)
in primary carbon	0.000	0.005 (0.0001)	0.009 (0.0003)	0.019 (0.0005)	0.040 (0.0004)
Ageing timescale of primary carbon (days)	N/A	0.24 (0.005)	0.44 (0.015)	0.96 (0.025)	2.08 (0.02)

1069

1070

1071

1072

1073 Table 3. Same as Table 2, except for POM budgets.

1074

	MAM3	MAM4L1	MAM4L2	MAM4L4	MAM4L8
Sources (Tg/yr)	50.2	50.2	50.2	50.2	50.2
Emission	50.2	50.2	50.2	50.2	50.2
Sinks (Tg/yr)	50.1 (0.064)	50.1 (0.041)	50.1 (0.053)	50.1 (0.037)	50.1 (0.044)
Dry deposition	7.5 (0.086)	8.1 (0.051)	8.4 (0.061)	9.0 (0.051)	10.0 (0.049)
Wet deposition	42.6 (0.089)	42.0 (0.071)	41.7 (0.063)	41.1 (0.078)	40.1 (0.051)
Lifetime (days)	4.34 (0.049)	4.62 (0.045)	4.96 (0.038)	5.69 (0.042)	7.02 (0.095)
Burden (Tg)	0.60 (0.007)	0.63 (0.006)	0.68 (0.005)	0.78 (0.006)	0.96 (0.013)
in accumulation	0.60 (0.007)	0.59 (0.006)	0.58 (0.005)	0.59 (0.004)	0.59 (0.009)
in primary carbon	0.00	0.049 (0.001)	0.097 (0.001)	0.19 (0.004)	0.37 (0.007)
Ageing timescale of primary carbon (days)	N/A	0.37 (0.008)	0.74 (0.008)	1.48 (0.03)	2.97 (0.06)

1075

1076

1077

1078 Table 4. Global BC budgets for resolution sensitivity simulations in set 2 experiments.
 1079

	MAM3R1	MAM4R2	MAM4R1	MAM4R0.5	MAM4R0.25
Sources (Tg/yr)	7.76	7.76	7.76	7.76	7.76
Emission	7.76	7.76	7.76	7.76	7.76
Sinks (Tg/yr)	7.75	7.75	7.75	7.75	7.74
Dry deposition	1.57	2.10	2.01	1.90	1.77
Wet deposition	6.18	5.65	5.74	5.85	5.97
Lifetime (days)	3.25	4.61	4.77	5.02	5.18
Burden (Tg)	0.069	0.098	0.101	0.107	0.110
in accumulation	0.069	0.064	0.068	0.071	0.076
in primary carbon	0.000	0.034	0.033	0.036	0.034
Ageing timescale of primary carbon (days)	N/A	1.80	1.73	1.88	1.77

1080

1081

1082

1083 Table 5. Same as Table 4, except for POM budgets.

1084

	MAM3R1	MAM4R2	MAM4R1	MAM4R0.5	MAM4R0.25
Sources (Tg/yr)	50.2	50.2	50.2	50.2	50.2
Emission	50.2	50.2	50.2	50.2	50.2
Sinks (Tg/yr)	50.1	50.1	50.2	50.1	50.1
Dry deposition	8.5	12.0	11.5	11.1	10.4
Wet deposition	41.6	38.1	38.6	39.1	39.7
Lifetime (days)	3.64	5.91	6.03	6.27	6.35
Burden (Tg)	0.50	0.81	0.83	0.86	0.87
in accumulation	0.50	0.48	0.50	0.52	0.55
in primary carbon	0.00	0.33	0.33	0.34	0.32
Ageing timescale of primary carbon (days)	N/A	2.68	2.66	2.73	2.56

1085

1086

1087

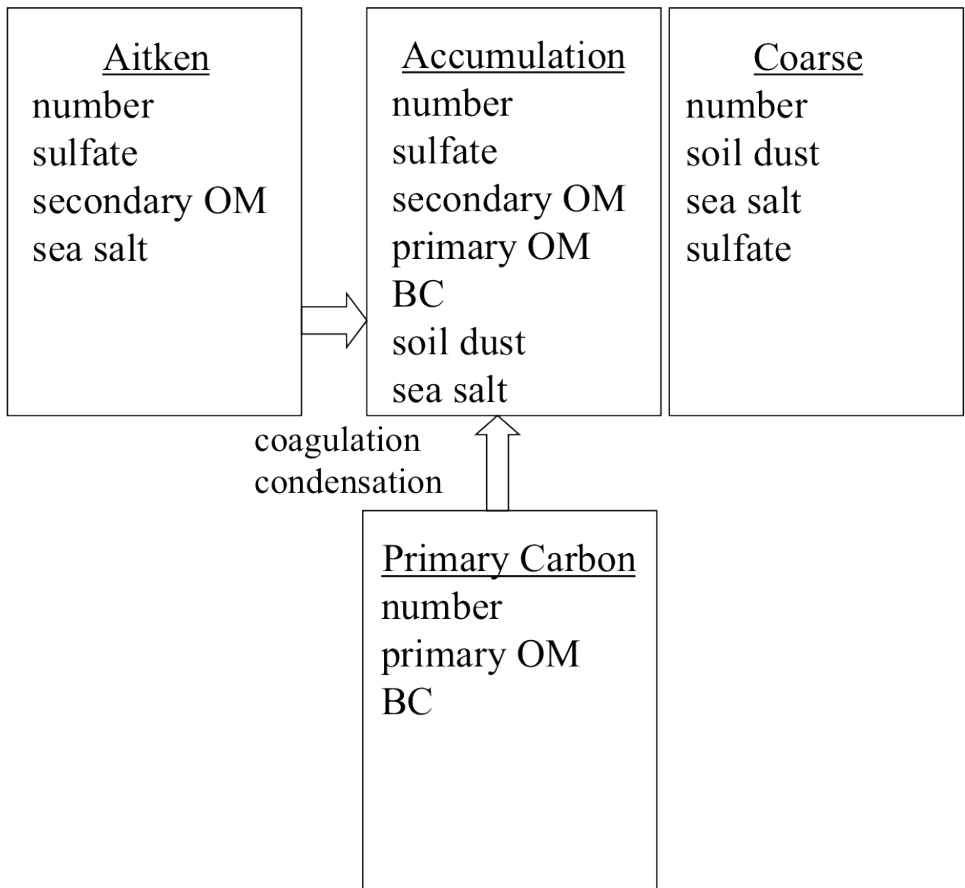


Fig. 1.

Column Burden

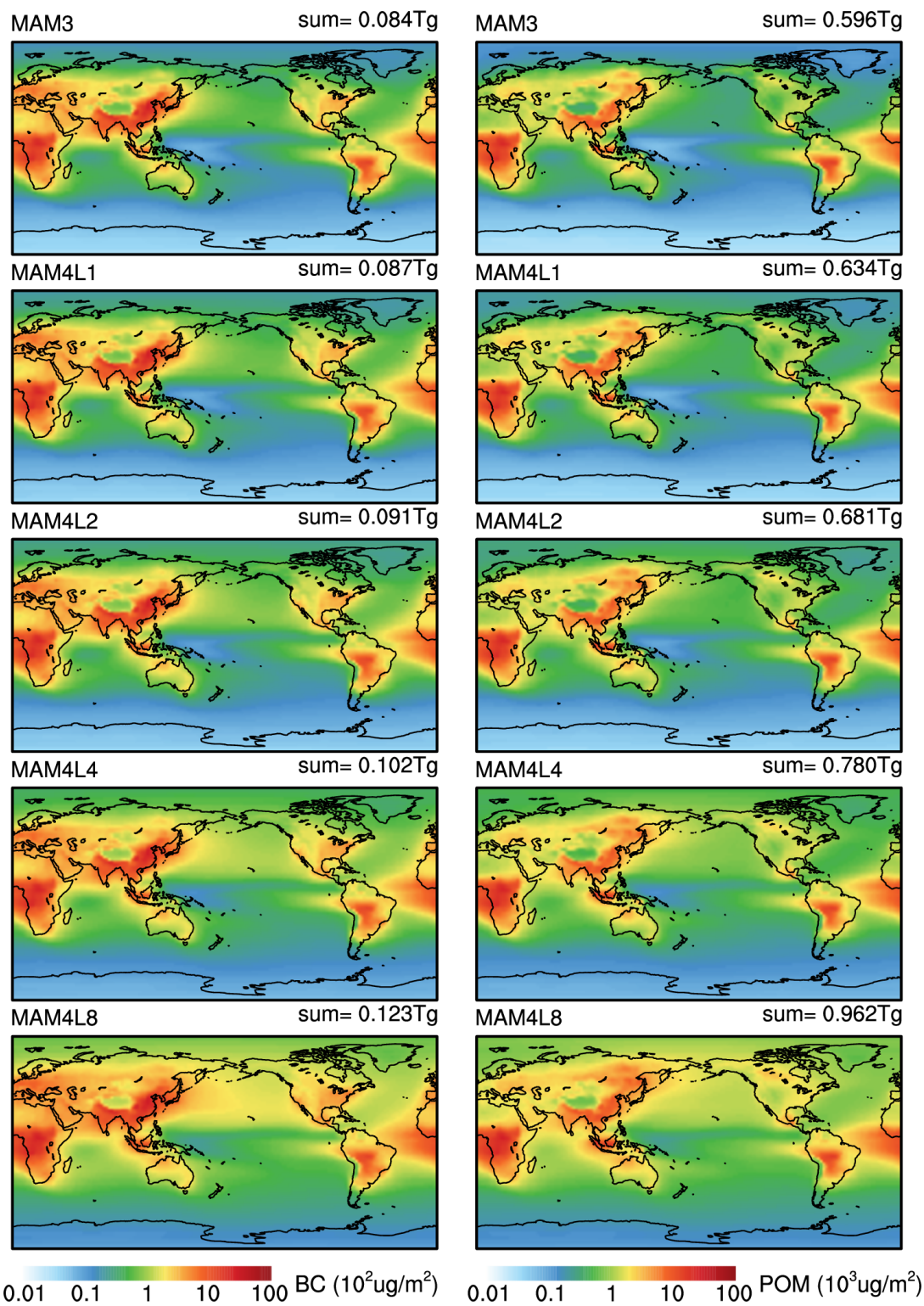


Fig. 2

Column Burden Difference Relative to MAM3

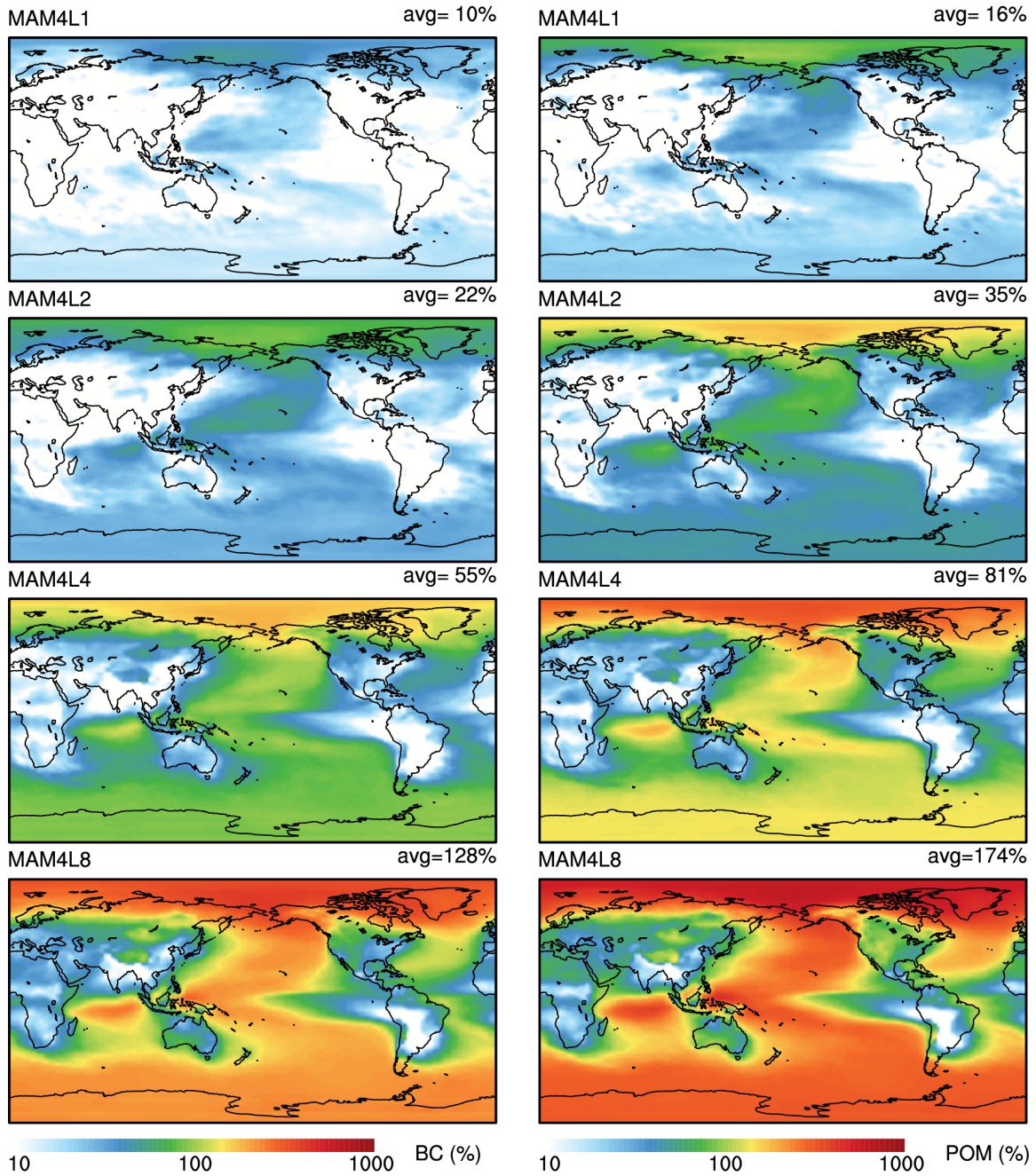


Fig.3

Column Burden

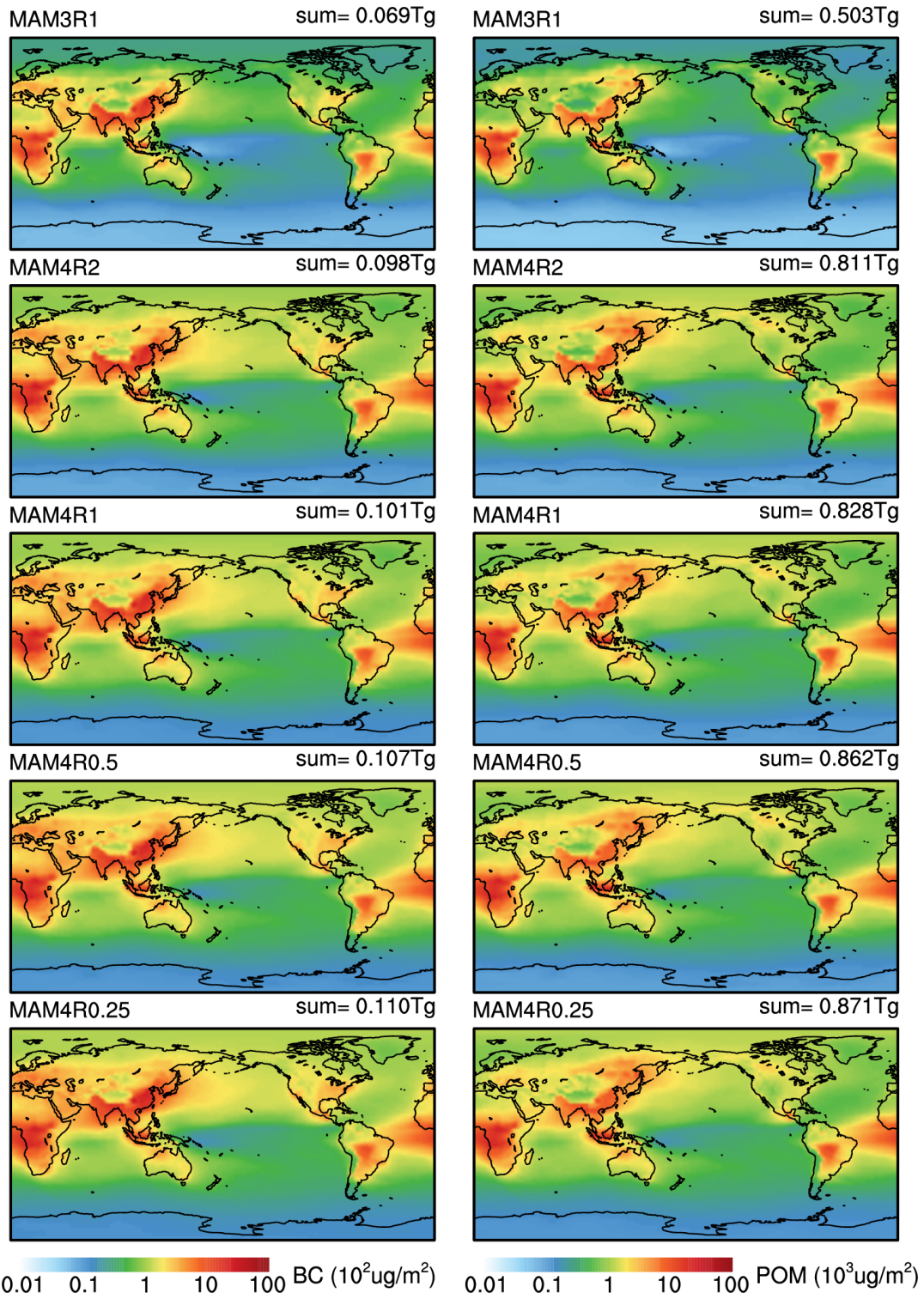


Fig. 4

Column Burden Difference Relative to MAM4R2

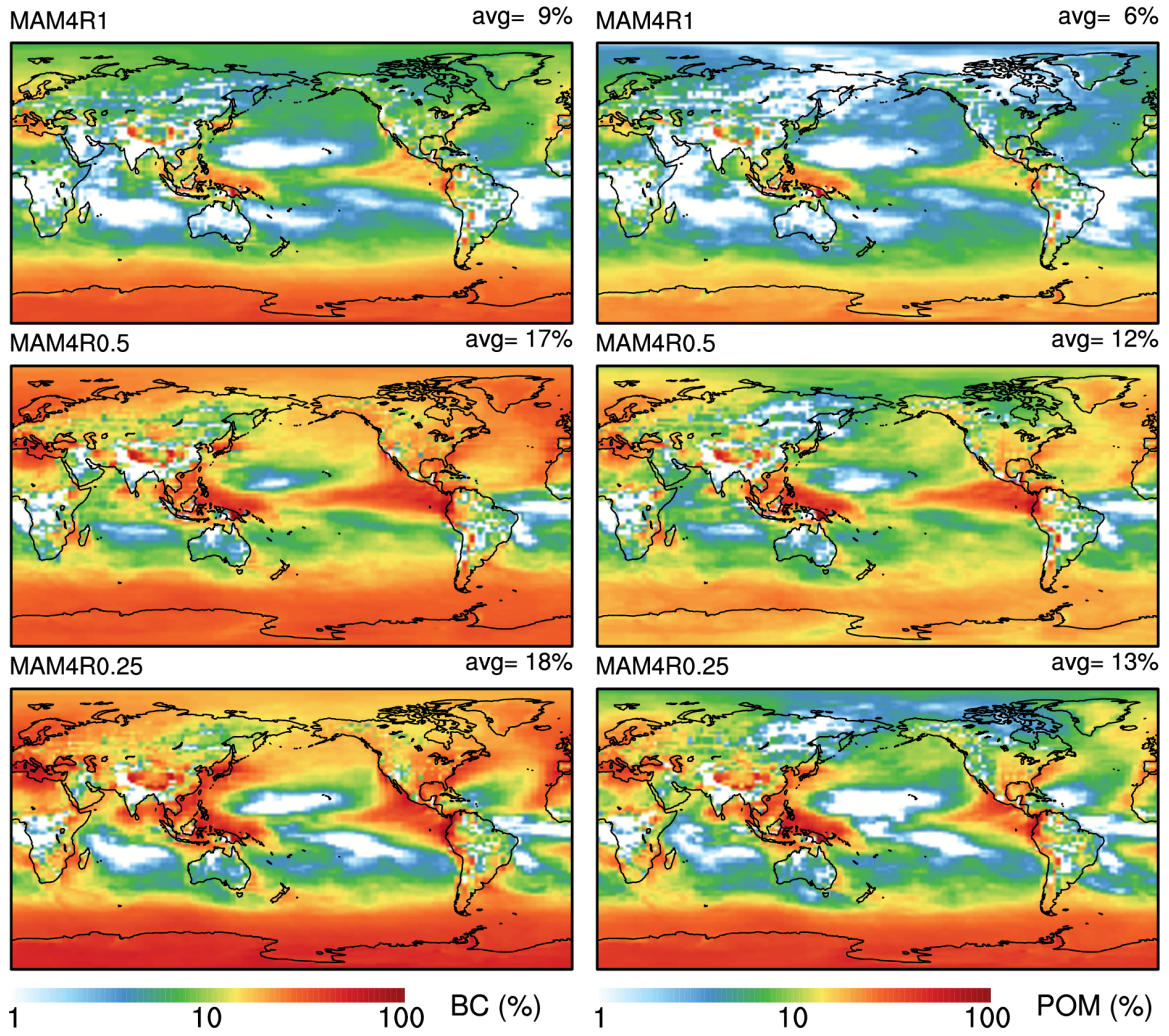
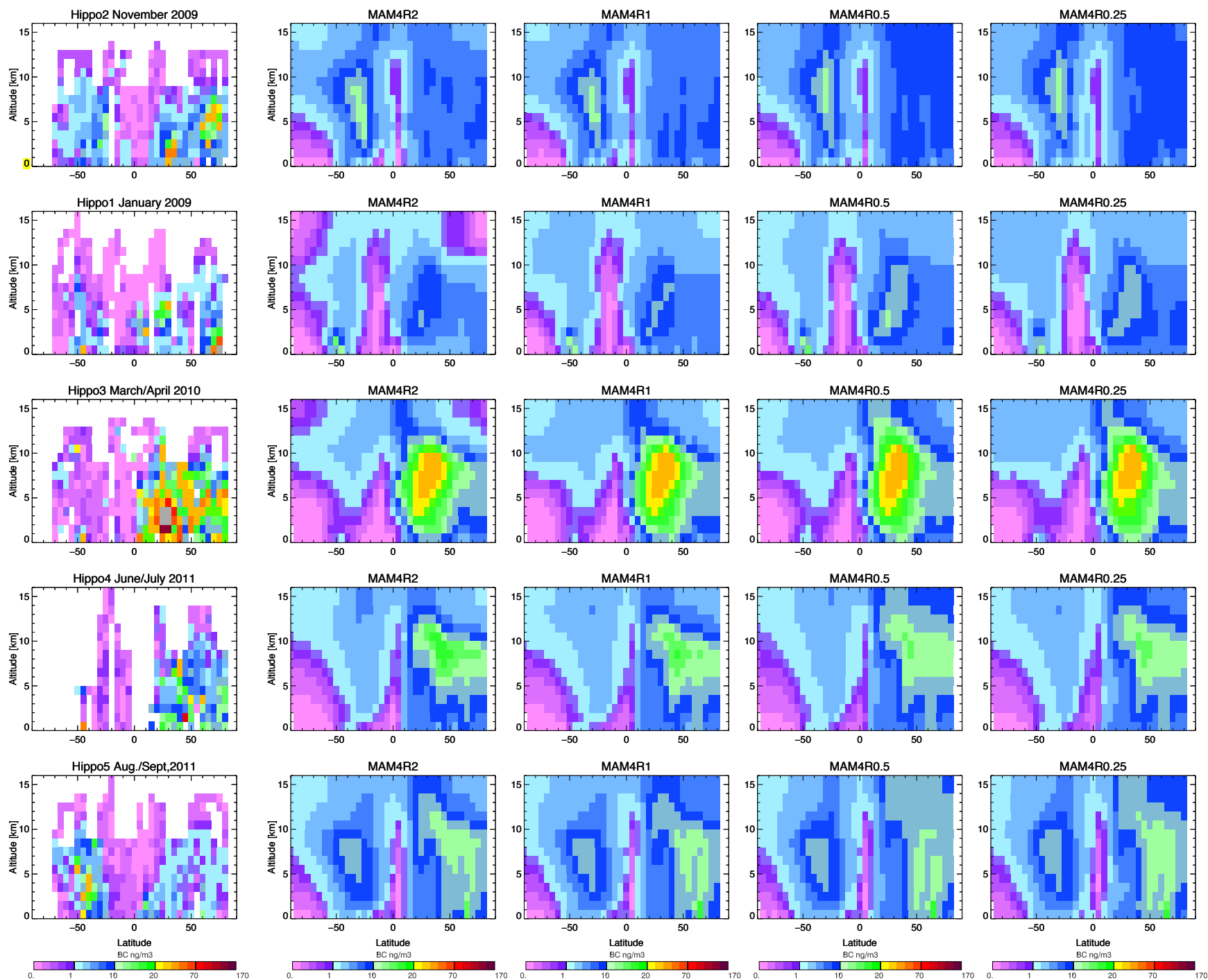


Fig. 5

Fig.6



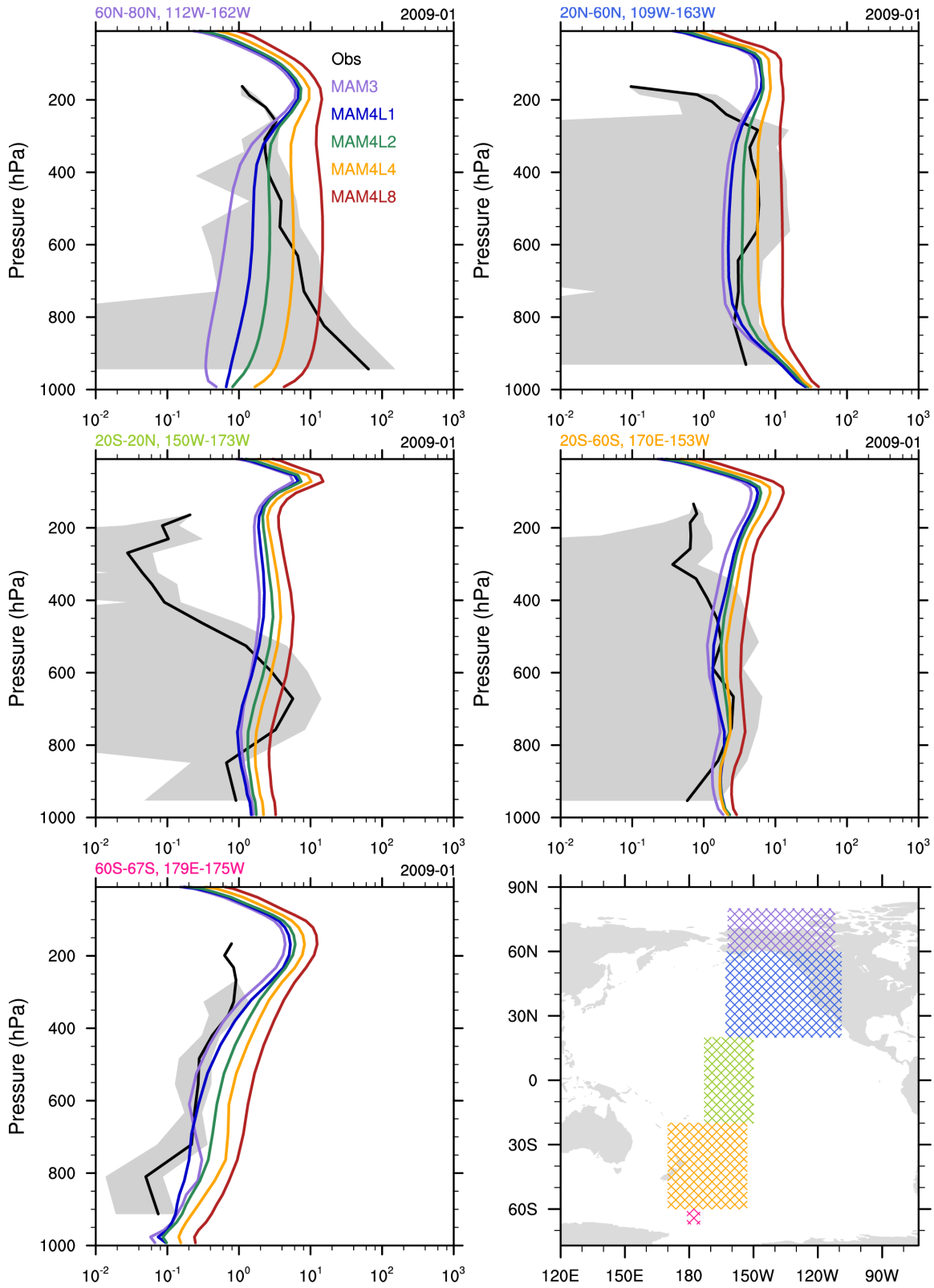


Fig. 7

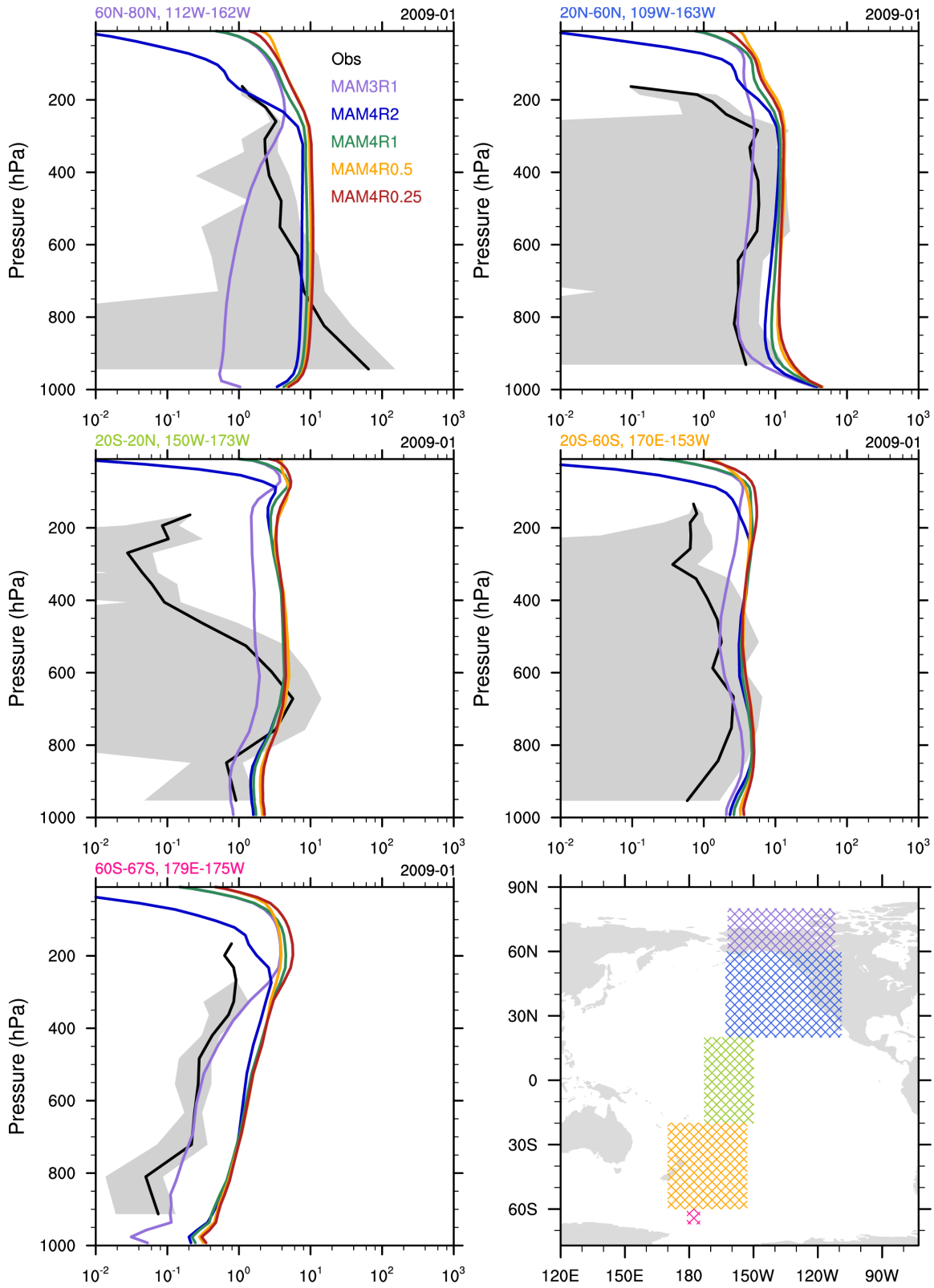


Fig.8

Fig. 9

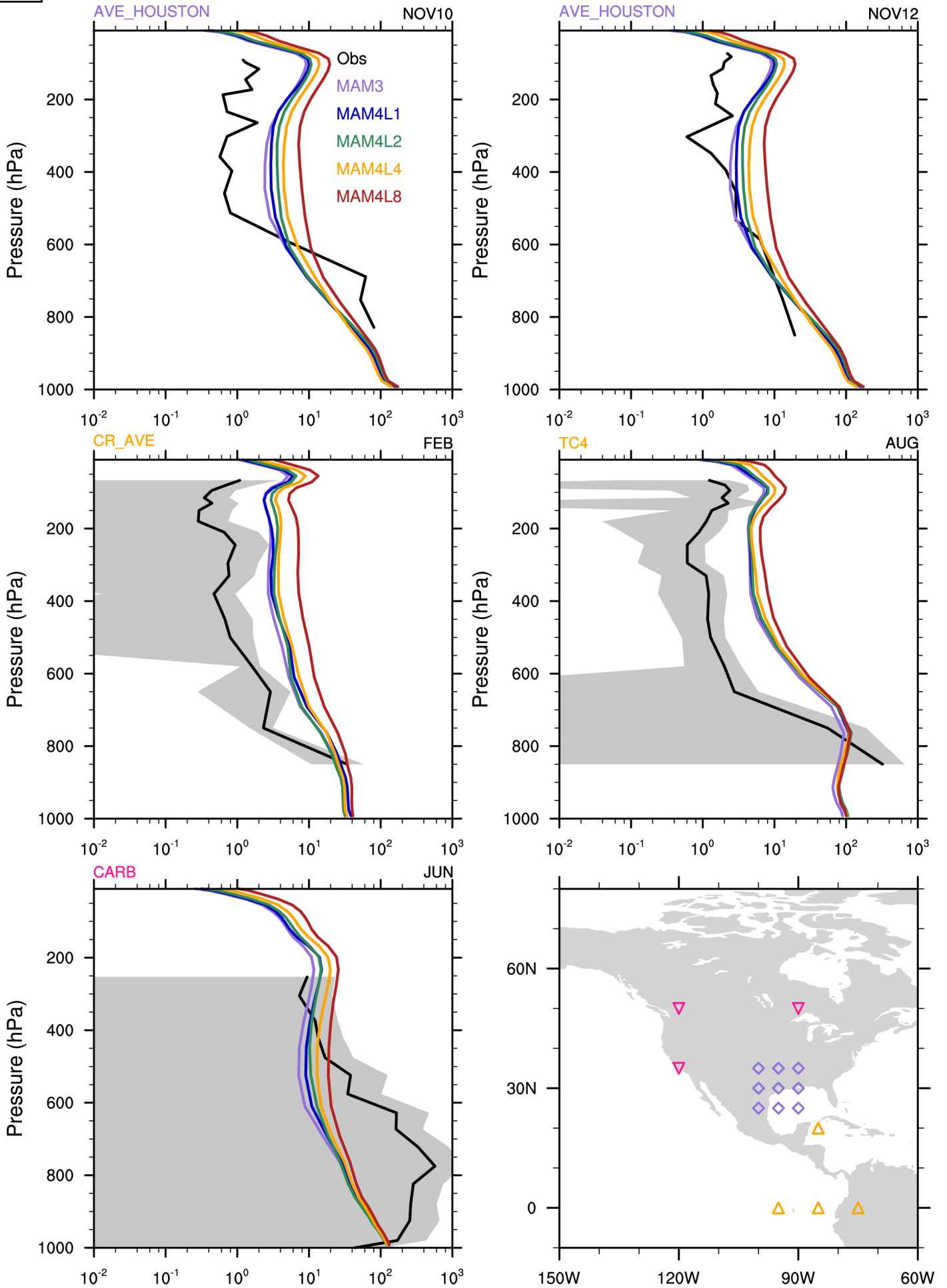


Fig.10

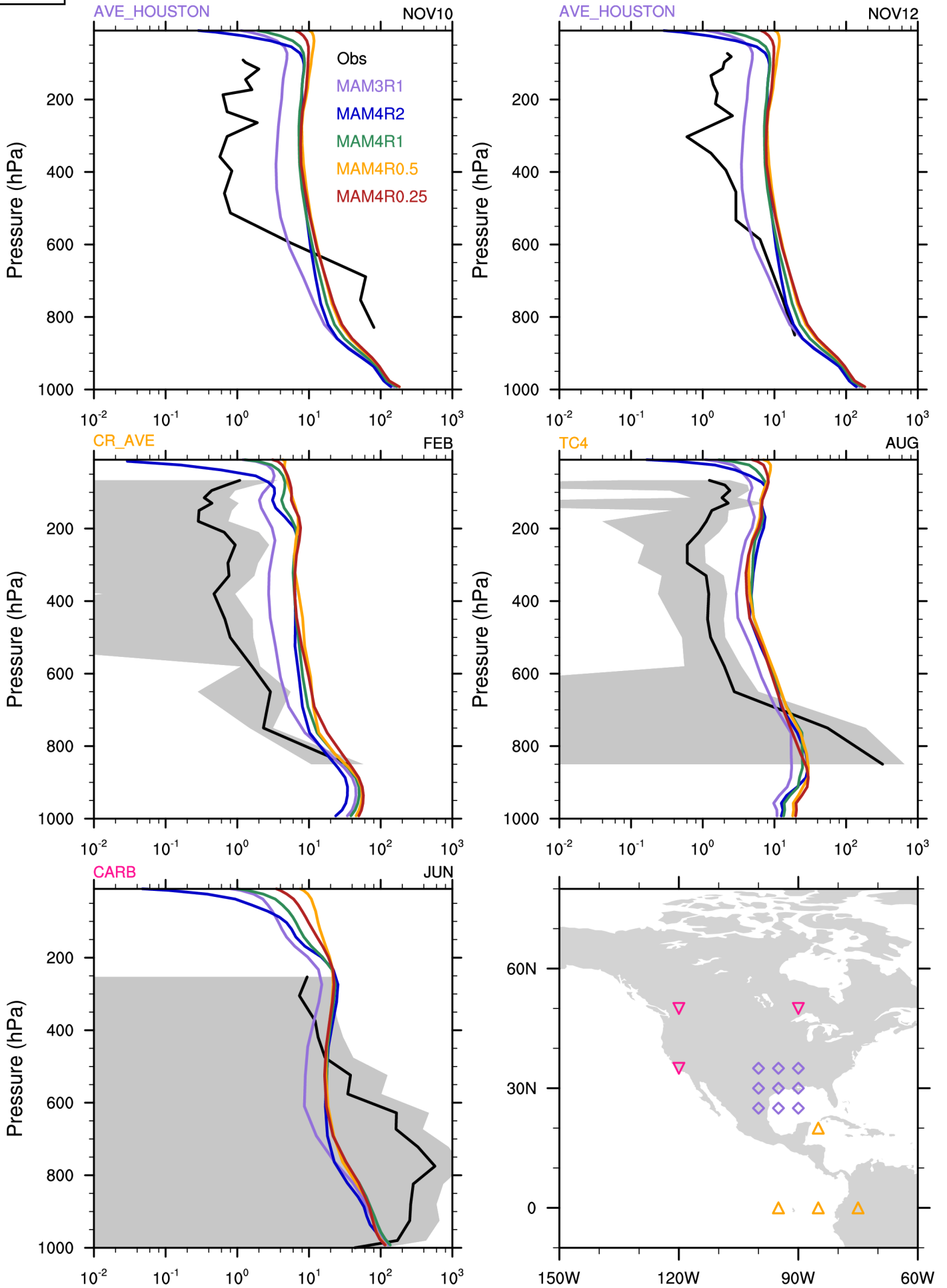


Fig. 11

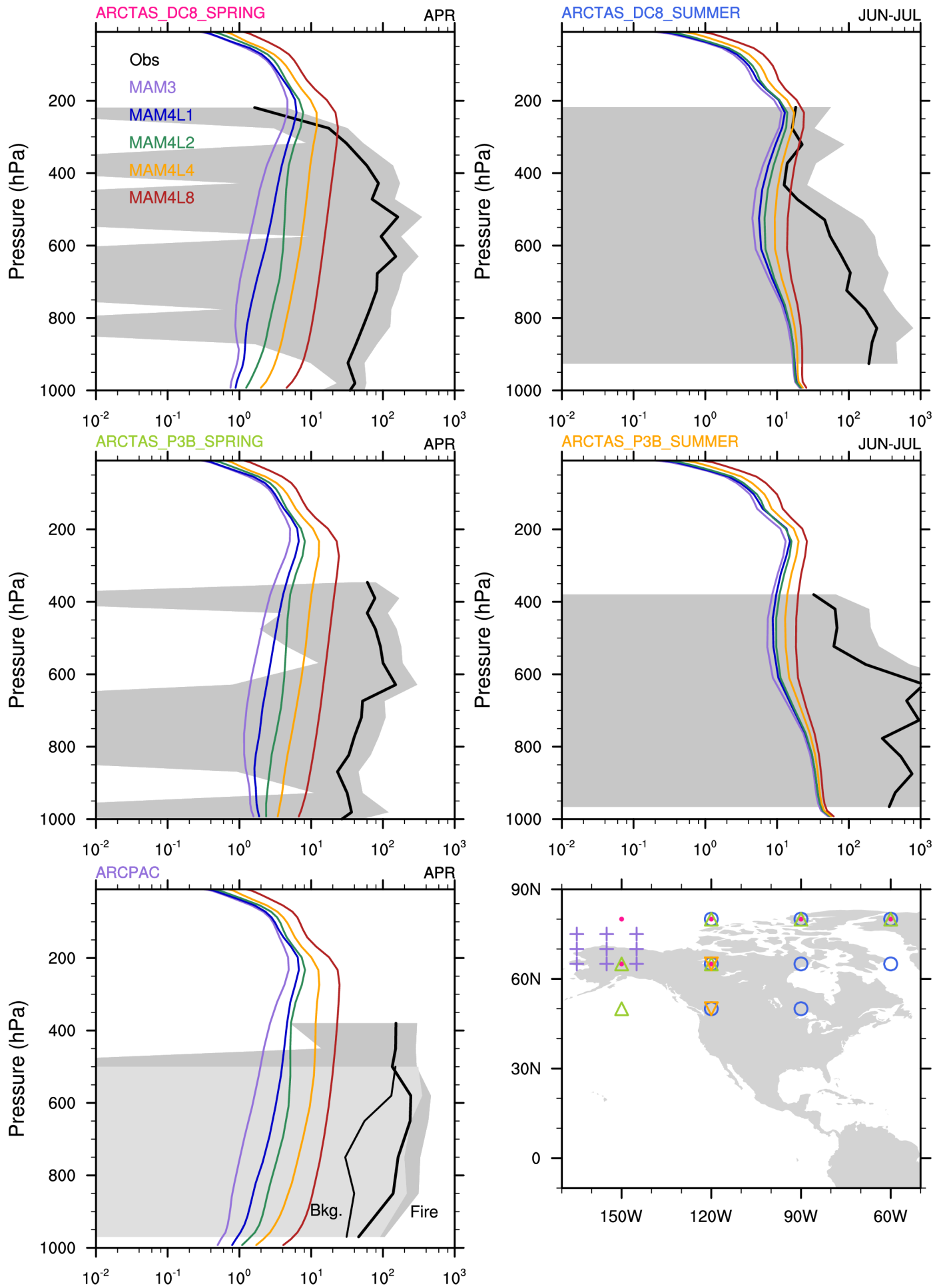


Fig.12

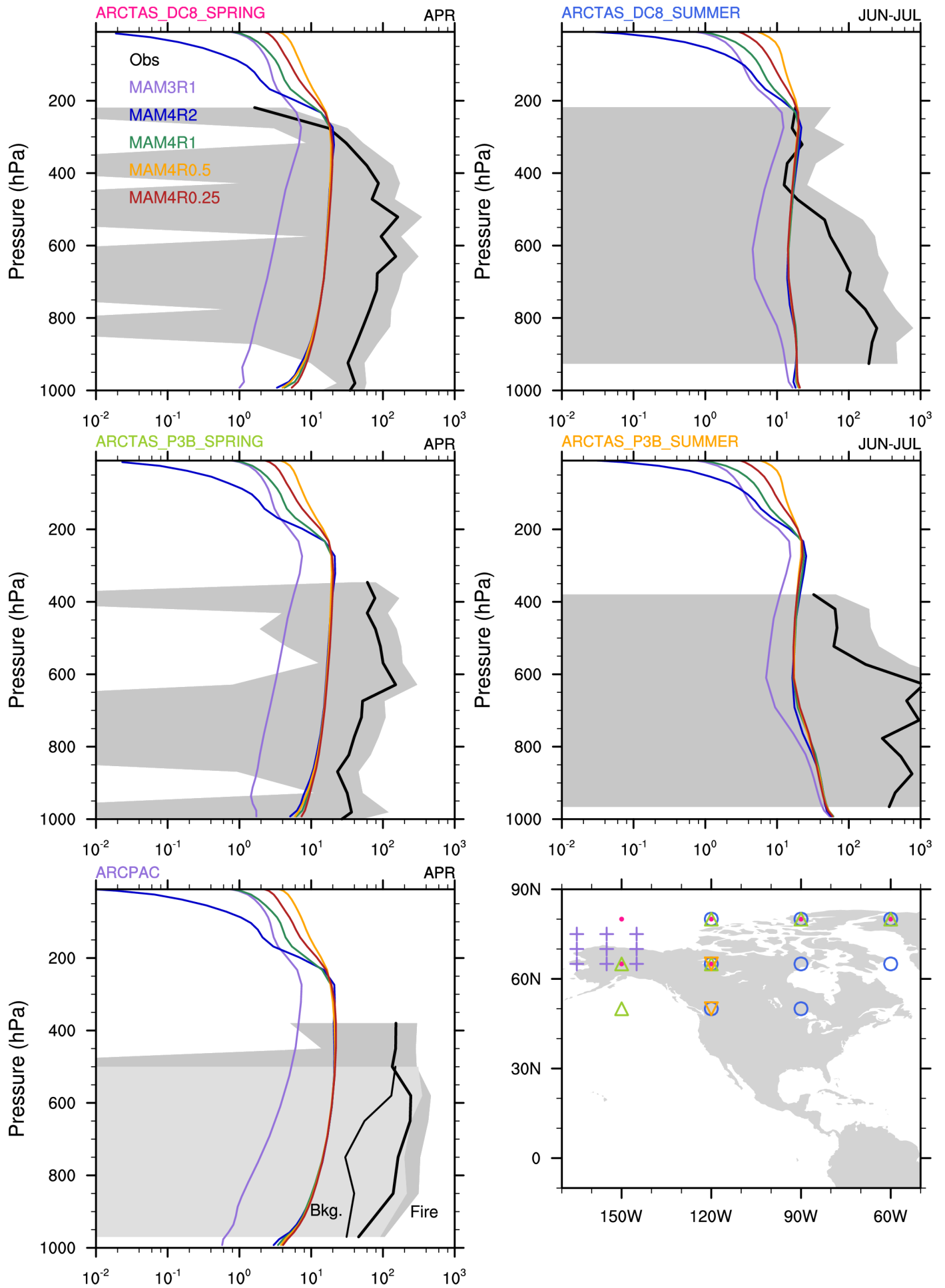


Fig.13

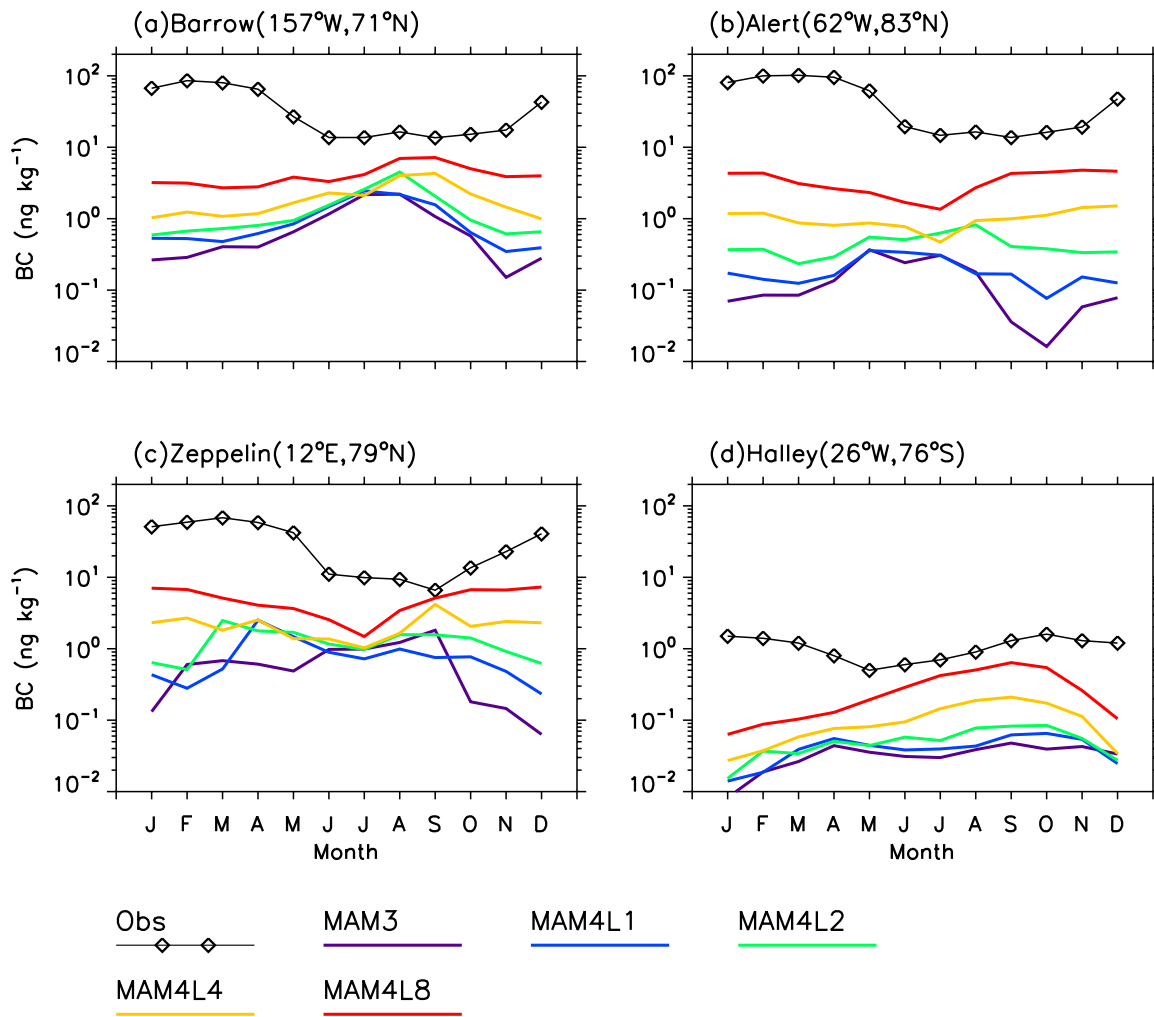


Fig.14

